

---

# BEYOND A SINGLE SIGNAL: SPECTRE-G2 – A UNIFIED MULTI-EXPERT ANOMALY DETECTOR FOR UNKNOWN UNKNOWNNS

---

**Rahul D Ray**

Department of Electronics and Electrical Engineering  
BITS Pilani, Hyderabad Campus  
f20242213@hyderabad.bits-pilani.ac.in

## ABSTRACT

Epistemic intelligence requires machine learning systems to recognise the limits of their own knowledge and to act safely under severe uncertainty, especially when faced with unknown unknowns—structural anomalies that violate the assumptions of the learned model. Existing uncertainty quantification methods typically rely on a single signal, such as confidence, density, or reconstruction error, and therefore fail to detect diverse types of structural violations. We introduce SPECTRE-G2, a multi-signal anomaly detector that combines eight complementary signals extracted from a dual-backbone neural network. The architecture comprises a spectral-normalised Gaussianization encoder, a plain MLP that preserves feature geometry, and an ensemble of five such encoders. From these we derive density, geometry, uncertainty, discriminative, and causal signals. Each signal is normalised using validation percentiles and its direction is corrected with a synthetic out-of-distribution set. An adaptive top- $k$  fusion selects the most discriminative signals per test set, averaging their normalised scores to produce a final anomaly score. Extensive experiments on four diverse datasets—synthetic causal, Adult, CIFAR-10, and Gridworld—show that SPECTRE-G2 achieves the highest mean AUROC on 11 out of 12 anomaly types and outperforms 12 strong baselines on AUPR, FPR95, and confident error rate. An ablation study confirms the robustness of the design: removing any single component causes only a minor performance drop, while the fusion of multiple signals is essential for high performance. The model exhibits stable results across random seeds and demonstrates particular strength on high-dimensional data and tasks requiring detection of new variables and confounders. SPECTRE-G2 thus provides a practical, principled solution for epistemic intelligence, enabling systems to detect unknown unknowns and to act safely in open-world environments.

## 1 Introduction

The deployment of machine learning systems in safety-critical domains such as autonomous driving, medical diagnosis, and industrial monitoring demands not only high predictive accuracy but also the ability to recognise when a model’s knowledge is insufficient. This capability, often termed *epistemic intelligence*, requires a system to quantify its own uncertainty and, crucially, to detect inputs that lie outside its training distribution—so-called *unknown unknowns* Burton and Herd [2023]. Unlike aleatoric uncertainty, which stems from inherent noise in the data, epistemic uncertainty arises from a lack of knowledge about the model’s parameters or about the correct model structure itself Fakour et al. [2024]. Distinguishing these two forms of uncertainty is essential for reliable decision making, especially when the system encounters novel scenarios that were not represented during training Miller [2021].

Early work on novelty detection already recognised the importance of identifying new or unknown data Markou and Singh [2003]. In recent years, the field of open-set recognition has formalised the problem of classifying known classes while rejecting inputs from unknown classes Pires et al. [2020]. A key insight is that epistemic uncertainty, rather than total predictive uncertainty, is the more informative signal for out-of-distribution (OOD) detection Everett et al. [2022], Oh et al. [2022]. For deep neural networks, epistemic uncertainty can be approximated by the mutual information of

an ensemble, a measure that has been shown to vastly outperform predictive entropy for OOD detection Everett et al. [2022].

A wide array of methods have been proposed to quantify epistemic uncertainty. Deep ensembles and Monte Carlo dropout approximate the posterior distribution over model parameters. Evidential deep learning models second-order uncertainty by placing a Dirichlet prior over class probabilities, allowing the network to “admit what it does not know” Ulmer et al. [2021]. Deterministic uncertainty methods such as DUQ use radial basis functions to achieve high-quality uncertainty estimates with a single forward pass. Conformal prediction provides distribution-free prediction sets with guaranteed coverage, and variants like entropy-based conformal scores have been used for OOD detection. Distance-based detectors, such as Mahalanobis OOD, and discriminative approaches like Outlier Exposure, further enrich the toolbox for identifying unknown inputs.

Several comprehensive surveys have synthesised this literature. Ruff et al. [2021] provide a unifying review of deep and shallow anomaly detection, highlighting that the detection of “unknown unknowns” is a strong driving force in the sciences. Pang et al. [2021] survey deep anomaly detection methods and identify “unknown anomaly detection” as a critical yet largely unsolved challenge. Gaudreault and Branco [2024] systematically review novelty detection in data streams, distinguishing novelty from outlier detection. Liso et al. [2024] focus on deep learning-based anomaly detection in Industry 4.0, covering applications in autonomous vehicles and sensor networks. Kumari et al. [2024] provide a comprehensive investigation of anomaly detection methods from 2019 to 2023, categorising approaches into machine learning, deep learning, and federated learning, and emphasising the challenge posed by the unknown nature of anomalies.

Despite this diversity, most existing methods rely on a single signal—confidence, density, reconstruction error, or a single uncertainty estimate—and therefore fail to capture the full spectrum of structural anomalies. The problem is compounded by the fact that unknown unknowns can take many forms: unobserved confounders, changed causal mechanisms, previously unseen variables, or novel interactions. In particular, the causal structure of the data generating process is often ignored, even though violations of that structure are a primary source of epistemic uncertainty.

To address these limitations, we propose SPECTRE-G2, a multi-signal anomaly detector that combines eight complementary signals extracted from a dual-backbone neural network. The architecture comprises a spectral-normalised Gaussianization encoder, a plain MLP that preserves feature geometry, and an ensemble of five such encoders. From these we derive density, geometry, uncertainty, discriminative, and causal signals. Each signal is normalised using validation percentiles and its direction is corrected with a synthetic out-of-distribution set. An adaptive top- $k$  fusion selects the most discriminative signals per test set, averaging their normalised scores to produce a final anomaly score.

Our contributions are threefold:

1. We introduce a principled multi-signal framework that integrates density, geometry, epistemic uncertainty, and causal consistency into a single anomaly score.
2. We present a dual-backbone design that resolves the trade-off between feature space stability (spectral normalisation) and geometry preservation (plain MLP), enabling both density-based and distance-based signals to be effective.
3. Through extensive experiments on four diverse datasets—synthetic causal, Adult, CIFAR-10, and Gridworld—we demonstrate that SPECTRE-G2 achieves state-of-the-art performance, winning on 11 out of 12 anomaly types and outperforming 12 strong baselines across AUROC, AUPR, and FPR95.

The remainder of this paper is organised as follows. Section 3 describes the datasets and the injection of structural anomalies. Section 4 reviews the twelve baseline methods. Section 5 details the architecture and mathematical formulation of SPECTRE-G2. Section 6 presents the experimental results, including a multi-seed evaluation and an ablation study. Section 8 discusses the implications, limitations, and future directions. Finally, Section 9 concludes the paper.

## 2 Related Work

This section reviews the extensive body of literature on uncertainty quantification and anomaly detection, covering surveys, ensemble methods, Bayesian approximations, evidential deep learning, conformal prediction, distance-based out-of-distribution (OOD) detection, and multi-signal causal approaches. The review highlights the diversity of existing methods and the gap that our proposed SPECTRE-G2 aims to fill.

## 2.1 Surveys and Foundational Reviews

The field of uncertainty in machine learning has been systematically surveyed in several recent works. Fakour et al. [2024] provide a structured review of uncertainty sources, categories (aleatoric vs. epistemic), and metrics for quantifying uncertainty in both single samples and datasets. Burton and Herd [2023] examine the role of uncertainty in the safety assurance of machine-learning systems, identifying typical weaknesses in assurance arguments. Markou and Singh [2003] present an early state-of-the-art review of novelty detection using statistical and neural approaches, noting the extreme difficulty of the task and its critical applications. Ruff et al. [2021] offer a unifying perspective on deep and shallow anomaly detection, connecting classic methods with modern deep learning techniques and emphasising the detection of “unknown unknowns” as a driving force. Pang et al. [2021] survey deep anomaly detection with a comprehensive taxonomy, highlighting the intrinsic challenges of handling unpredictable and rare events. Gaudreault and Branco [2024] systematically review novelty detection in data streams, distinguishing it from outlier detection. Liso et al. [2024] focus on deep learning-based anomaly detection in Industry 4.0, covering applications such as autonomous vehicles. Kumari et al. [2024] provide a wide-ranging investigation of anomaly detection methods from 2019 to 2023, categorising them into machine learning, deep learning, and federated learning. Finally, Gao et al. [2025] survey evidential deep learning (EDL), detailing its theoretical foundations in subjective logic and its applications.

## 2.2 Ensemble and Bayesian Uncertainty Methods

Ensemble techniques are a powerful way to estimate uncertainty. Lakshminarayanan et al. [2017] proposed deep ensembles, which train several independent networks and average their predictions; they demonstrated that ensembles often outperform approximate Bayesian methods. Nguyen et al. [2021] compared Monte Carlo dropout (MCDO) and bootstrap aggregation (bagging) for radiation therapy dose prediction, finding that bagging yields lower error and comparable uncertainty estimates. Qendro et al. [2021] introduced early-exit ensembles, which provide better-calibrated uncertainty than both MCDO and deep ensembles. Durasov et al. [2021] analysed why MCDO underperforms relative to ensembles, attributing it to high correlation between predictions. Pop and Fulop [2018] combined ensembles with MCDO in the Deep Ensemble Bayesian Active Learning (DEBAL) framework, showing improved uncertainty estimates. Zhang et al. [2019] proposed structured dropout for confidence calibration. Everett et al. [2022] demonstrated that epistemic uncertainty, approximated by mutual information, vastly outperforms total uncertainty for OOD detection, and introduced adversarial training to further improve performance. Oh et al. [2022] used the inherent epistemic uncertainty of a pre-trained model to enhance OOD detection via the UA-FGSM algorithm.

## 2.3 Evidential Deep Learning

Evidential deep learning (EDL) models second-order uncertainty by treating network outputs as parameters of a Dirichlet distribution. Sensoy et al. [2018] introduced the original EDL framework, which enables a single deterministic network to quantify both aleatoric and epistemic uncertainty. Ulmer et al. [2021] surveyed prior and posterior networks, discussing how EDL allows a network to fall back on a uniform prior for unknown inputs. Schreck et al. [2024] compared EDL with ensembles in Earth system science applications, finding that EDL achieves comparable accuracy while robustly estimating uncertainties. Juergens et al. [2024] critically examined whether EDL faithfully represents epistemic uncertainty, concluding that while it provides useful relative measures, quantitative faithfulness is not guaranteed. Aguilar et al. [2023] integrated EDL into a continual learning framework for simultaneous incremental classification and OOD detection, achieving strong results on CIFAR-100.

## 2.4 Conformal Prediction

Conformal prediction (CP) provides distribution-free prediction sets with guaranteed coverage. Novello et al. [2024] explored the interplay between OOD detection and CP, showing that OOD scores can serve as nonconformity measures. Garg and Majumder [2025] proposed BaKC+, which combines cross-conformal prediction with ensembles and sampling for one-class anomaly detection. Katsios and Papadopoulos [2024] introduced a Mahalanobis distance nonconformity measure for multi-label CP, improving informational efficiency. Nanopoulos and Buza [2025] addressed OOD time-series classification using CP with label smoothing and hybrid classifiers. Karzanov and Detyniecki [2026] developed Geometrically Constrained Outlier Synthesis (GCOS), a training-time regularisation that integrates with CP for OOD inference. Peng et al. [2025] proposed a detect-then-impute conformal prediction framework to handle cellwise outliers in test features.

## 2.5 Distance-Based and Causal Methods

Distance-based detectors are a classic approach to OOD detection. Karzanov and Detyniecki [2026] used the Mahalanobis distance as a score space for contrastive regularisation. Several recent works incorporate causal reasoning into anomaly detection. Tang et al. [2023] proposed causality-guided counterfactual debiasing for cyber-physical systems. Malarkkan et al. [2024] fused multi-view causal graphs for anomaly detection in infrastructures. Simanek et al. [2015] improved multi-modal data fusion via anomaly detection. Xing et al. [2025] used a dual-channel deep learning approach with causal inference for microservice anomaly detection. Moldovan and Iantovics [2025] reviewed information fusion-based data mining for complex anomaly detection. Zhang et al. [2021] proposed unsupervised deep anomaly detection for multi-sensor time-series signals. Gu et al. [2025] introduced multi-modal contrastive causal consistency fusion for additive manufacturing anomaly detection.

## 2.6 Multi-Signal Fusion and Open-Set Recognition

The idea of combining multiple signals to improve detection is not new. Pires et al. [2020] proposed knowledge uncertainty estimation (KUE) for open-set recognition, using ensemble entropy to distinguish aleatoric from epistemic uncertainty. Miller [2021] explored epistemic uncertainty estimation for object detection in open-set conditions, establishing open-set object detection as a task. Liu et al. [2026] proposed a bearing anomaly detection method based on multimodal fusion and self-adversarial learning. These works, together with the surveys and methods above, illustrate that existing approaches typically rely on a single uncertainty signal (e.g., ensemble variance, entropy, Mahalanobis distance). Our work, SPECTRE-G2, differs by fusing eight complementary signals—density, geometry, epistemic uncertainty, discriminative confidence, and causal residuals—into a single adaptive score. This multi-signal fusion, combined with a dual-backbone architecture that balances stability and geometry, addresses the challenge of detecting diverse unknown unknowns that no single signal can capture reliably.

## 3 Benchmark Datasets and Preprocessing

To rigorously evaluate the performance of uncertainty quantification methods under known and unknown structural violations, we construct a benchmark comprising four distinct datasets. Each dataset captures a different data modality—synthetic causal, tabular, image, and reinforcement learning—and includes a training set representing the “normal” distribution, together with several test sets that introduce specific types of unknown unknowns. All datasets are generated with fixed random seeds to ensure reproducibility, and preprocessing steps are applied consistently across all models.

### 3.1 Synthetic Causal Dataset

The synthetic dataset is built around a known causal directed acyclic graph (DAG) that defines the relationships among six continuous variables. The graph structure is:

$$X_1 \rightarrow X_2, X_1 \rightarrow X_3, X_2 \rightarrow X_4, X_3 \rightarrow X_5, X_4 \rightarrow Y, X_5 \rightarrow Y.$$

The functional forms are a mixture of linear and non-linear transformations with additive Gaussian noise:

$$\begin{aligned} X_1 &\sim \mathcal{N}(0, 1), \\ X_2 &= 0.8 X_1 + \epsilon_2, \quad \epsilon_2 \sim \mathcal{N}(0, 0.3), \\ X_3 &= -0.5 X_1 + 0.4 X_1^2 + \epsilon_3, \quad \epsilon_3 \sim \mathcal{N}(0, 0.3), \\ X_4 &= 0.7 X_2 + \epsilon_4, \quad \epsilon_4 \sim \mathcal{N}(0, 0.3), \\ X_5 &= \tanh(0.9 X_3) + \epsilon_5, \quad \epsilon_5 \sim \mathcal{N}(0, 0.3), \\ Y &= 0.6 X_4 + 0.5 X_5 + 0.3 X_1 + \epsilon_Y, \quad \epsilon_Y \sim \mathcal{N}(0, 0.3). \end{aligned}$$

The training set consists of 10 000 samples drawn from this base distribution. The regular test set (2 000 samples) is sampled identically and serves as the in-distribution reference.

To simulate different kinds of unknown unknowns, we generate four additional test sets, each containing 2 000 samples, by introducing structural perturbations not present during training:

- **Confounder:** An unobserved variable  $U \sim \mathcal{N}(0, 1)$  influences both  $X_2$  and  $X_4$ :

$$X_2 = 0.8 X_1 + 0.6 U + \epsilon_2, \quad X_4 = 0.7 X_2 + 0.6 U + \epsilon_4.$$

This creates a spurious correlation that breaks the Markov property of the learned graph.

- **New variable:** A new observed variable  $X_6 \sim \mathcal{N}(0, 1)$  directly influences the target:

$$Y = Y_{\text{base}} + 0.8 X_6,$$

where  $Y_{\text{base}}$  is the original  $Y$  from the base distribution. This represents a previously unmodelled causal factor.

- **Changed mechanism:** The edge  $X_2 \rightarrow X_4$  is altered from linear to quadratic:

$$X_4 = 0.35 X_2^2 + \epsilon_4,$$

changing the conditional distribution of  $X_4$  given its parent.

- **Interaction:** An interaction term  $X_2 X_3$  is added to the target equation:

$$Y = Y_{\text{base}} + 0.5 X_2 X_3,$$

introducing a higher-order dependence not present in the training data.

All perturbations are designed to be subtle enough that they do not produce a simple distribution shift in the marginal densities of the observed variables, forcing detection methods to rely on structural consistency rather than mere density estimation.

### 3.2 Adult Dataset (UCI)

The Adult dataset is a classic tabular classification benchmark where the goal is to predict whether an individual’s annual income exceeds \$50K. After removing rows with missing values, we obtain 32 561 instances. The feature set includes both continuous and categorical attributes. We retain the continuous features: *age*, *education-num*, *hours-per-week*, *capital-gain*, and *capital-loss*. The categorical features *occupation* and *marital-status* are one-hot encoded, resulting in a total of 25 input dimensions. The target is binary. All continuous features are standardised using the mean and standard deviation computed from the training set.

From the original data, we create a training set (80% of the data) and a regular test set of 2 000 samples, drawn from the same distribution. To inject unknown unknowns, we construct three anomaly test sets, each also with 2 000 samples:

- **New variable:** A synthetic binary feature “inheritance” is generated based on age and education (with probability 0.3) and then used to flip the target for 20% of the cases where it is active. This mimics the effect of an unobserved hereditary factor.
- **Changed mechanism:** The influence of education on income is altered by randomly flipping the target for individuals whose *education-num* lies in the middle two quartiles (with probability 0.5), breaking the monotonic relationship observed in the training data.
- **Confounder:** A hidden binary variable “wealthy family” (probability 0.2) is introduced. It increases *education-num* by one and also flips the target for 35% of those affected, acting as a common cause that induces spurious dependence.

All anomalies are constructed so that the marginal distributions of the observed features remain largely unchanged, emphasising the need to detect changes in conditional relationships.

### 3.3 CIFAR-10 Image Dataset

For the image domain, we use the CIFAR-10 dataset, which contains 60 000 colour images of size  $32 \times 32$  across 10 classes. To obtain semantically meaningful features, we employ a pretrained ResNet-18 network (trained on ImageNet) as a fixed feature extractor, discarding the final classification layer. The output of the penultimate layer provides a 512-dimensional feature vector for each image. We randomly subsample the training set to 5 000 images and the regular test set to 1 000 images.

To create test sets with unknown unknowns, we apply image-level transformations that alter the causal relationship between the object class and the observed features, while preserving the class labels:

- **Changed mechanism:** The brightness of the image is inverted (pixel values are negated), simulating a drastic change in lighting that violates the assumed relationship between class and pixel intensities.
- **New variable:** A Gaussian blur (radius 1.5) is applied to the image, representing the introduction of a camera artefact that was not present during training.

- **Confounder:** For images belonging to odd-numbered classes, a red colour cast is added by increasing the red channel by 0.5. This mimics an unobserved time-of-day confounder that influences both the class distribution and the appearance.

After applying these transformations, the same frozen ResNet-18 is used to extract feature vectors, so that the anomaly test sets are represented in the same feature space as the training data. This setup tests the ability of uncertainty methods to detect when the class-to-feature mapping has been structurally altered.

### 3.4 Gridworld Reinforcement Learning Environment

The Gridworld environment is a custom  $10 \times 10$  grid where an agent moves by selecting one of four actions (up, down, left, right). The state consists of the agent’s coordinates  $(a_x, a_y)$ , the coordinates of an object  $(o_x, o_y)$ , and the proximity (inverse Euclidean distance) between them:

$$\text{proximity} = \frac{1}{1 + \sqrt{(a_x - o_x)^2 + (a_y - o_y)^2}}.$$

The reward depends on the object type (A or B) and the proximity according to a base reward function:

$$\text{reward} = \begin{cases} 1.5 \times \text{proximity}, & \text{if object} = \text{A}, \\ -1.0 \times \text{proximity}, & \text{if object} = \text{B}. \end{cases}$$

The training set is generated by random rollouts of 5 000 steps, and the regular test set contains 1 000 steps from the same distribution.

Two anomaly test sets are constructed:

- **New object:** A third object type C is introduced, with a reward function that gives a positive reward only for a specific range of proximity values:

$$\text{reward} = \begin{cases} 2.0, & \text{if } 0.3 < \text{proximity} \leq 0.7, \\ -0.5, & \text{otherwise.} \end{cases}$$

This simulates a previously unseen object type with a different reward structure.

- **Changed mechanism:** The reward functions for existing objects A and B are changed to step functions:

$$\text{reward}_A = \begin{cases} 2.0, & \text{if proximity} > 0.5, \\ 0.1, & \text{otherwise,} \end{cases} \quad \text{reward}_B = \begin{cases} -2.0, & \text{if proximity} > 0.5, \\ -0.1, & \text{otherwise.} \end{cases}$$

This alters the causal relationship between proximity and reward, requiring detection methods to recognise that the reward model has changed.

The Gridworld dataset is particularly useful for evaluating uncertainty in sequential decision-making, where an agent must recognise when the environment’s reward structure has been altered to avoid catastrophic mistakes.

### 3.5 Data Preprocessing and Splits

All datasets undergo a standardised preprocessing pipeline. Continuous features are standardised to zero mean and unit variance using the statistics of the training set only; the same scaling is applied to validation and test sets. For categorical variables (Adult), one-hot encoding is performed before standardisation. The training set is further split into an 80% training partition and a 20% validation partition, the latter used for early stopping and hyperparameter selection. The regular test set (in-distribution) is used to establish a baseline for the anomaly detection metrics. The anomaly test sets are presented to all models without any indication of the type of anomaly, ensuring a fair evaluation of their ability to detect unknown unknowns.

The four datasets were chosen to cover a wide spectrum of data types and structural anomalies. The synthetic dataset provides a ground-truth causal graph, allowing us to precisely control the types of structural violations and to evaluate whether methods can detect deviations from the learned causal structure. The Adult dataset represents a realistic, noisy tabular classification task where anomalies are injected in a semi-synthetic manner that preserves marginal distributions. The CIFAR-10 dataset tests high-dimensional perceptual data, where the anomalies are induced by image transformations that alter the relationship between class and features without changing the class labels. Finally, the Gridworld environment offers a sequential decision-making setting where the reward structure can be changed, testing the robustness of uncertainty quantification in reinforcement learning. By evaluating across these diverse domains, we can assess the generalisability of different uncertainty quantification approaches and their ability to recognise when the underlying causal model is no longer valid.

## 4 Baseline Methods for Uncertainty Quantification

To provide a comprehensive evaluation of epistemic uncertainty and anomaly detection, we implement twelve baseline methods, each representing a distinct paradigm for quantifying uncertainty. These methods span ensemble-based, Bayesian, evidential, deterministic, conformal, discriminative, and distance-based approaches. All baselines share a common architectural backbone: a three-layer multilayer perceptron (MLP) with 128 hidden units per layer, ReLU activations, and a dropout rate of 0.2 (except where noted). The same training protocol is applied uniformly: 30 epochs, Adam optimiser with learning rate  $10^{-3}$ , cosine annealing learning rate schedule, and early stopping on validation cross-entropy loss with a patience of 5 epochs. For stochastic methods, 30 Monte Carlo samples are used at test time. All results are reported as means over 5 independent random seeds.

### 4.1 Deep Ensembles

Deep Ensembles train multiple independent neural networks with the same architecture but different random initialisations. Here we use five such networks. At inference, the predictions of all networks are averaged to produce a final probability distribution. The maximum value of this average is taken as a confidence score. The intuition is that in-distribution samples will be predicted consistently across the ensemble, yielding high confidence, while out-of-distribution or structurally anomalous inputs will cause disagreement, leading to lower confidence. The negative of this confidence is used as an anomaly score.

### 4.2 Monte Carlo Dropout

Monte Carlo Dropout approximates Bayesian inference by applying dropout at test time. A single MLP is trained with dropout regularisation (dropout probability 0.3). At inference, 30 forward passes are performed with dropout enabled, sampling from an approximate posterior over the weights. The predictions are averaged across these passes to obtain a final probability vector, and its maximum is used as the confidence score. The negative of this confidence serves as the anomaly score. This method captures model uncertainty through the variance of the stochastic passes.

### 4.3 Bayesian Neural Network via Last-Layer Laplace Approximation

This implementation approximates the posterior over the final layer weights using a Laplace approximation. After training a standard MLP (without dropout), the penultimate layer activations are extracted for the entire training set. A logistic regression model with  $\ell_2$  regularisation is then fitted to these features, using the true class labels. This logistic model provides predictive probabilities that incorporate uncertainty in the linear decision boundary. For a test input, the penultimate features are extracted from the trained MLP, and the logistic model produces the final probability. The maximum of this probability is used as the confidence score, and its negative as the anomaly score.

### 4.4 Bayesian Entropy Neural Network

Bayesian Entropy Neural Networks augment MC Dropout with a maximum-entropy regularisation term during training. The loss function combines cross-entropy with a penalty that encourages the softmax outputs to be uniform, preventing over-confidence. The penalty is proportional to the mean entropy of the batch’s softmax outputs. At test time, 30 stochastic forward passes with dropout are performed and averaged. The confidence score is the maximum of the averaged probability, and the anomaly score is its negative.

### 4.5 Evidential Deep Learning

Evidential Deep Learning treats the network’s outputs as parameters of a Dirichlet distribution over class probabilities. The final layer produces evidence values, passed through a softplus activation to ensure positivity. The evidence for each class is transformed into Dirichlet concentration parameters  $\alpha_k = e_k + 1$ . The loss encourages the Dirichlet distribution to concentrate on the true class while penalising evidence assigned to incorrect classes. At inference, the predicted probability for class  $k$  is  $\alpha_k / \sum_j \alpha_j$ , and the uncertainty (vacuity) is defined as  $K / \sum_j \alpha_j$ , where  $K$  is the number of classes. This vacuity is used directly as the anomaly score; higher vacuity indicates a more uncertain input.

### 4.6 Deterministic Uncertainty Quantification with RBF

This method uses radial basis functions (RBFs) to compute distances to class centroids in a learned feature space. The network is split into a feature extractor (the first three layers of the MLP) and a head that produces RBF outputs. During training, a centroid for each class is maintained and updated via an exponential moving average of the feature vectors

belonging to that class. At test time, the output for class  $c$  is  $\exp\left(-\frac{\|\phi(\mathbf{x})-\mathbf{c}_c\|^2}{2\ell^2}\right)$ , where  $\phi(\mathbf{x})$  is the feature vector,  $\mathbf{c}_c$  is the centroid, and  $\ell$  is a fixed length scale. The confidence score is the maximum RBF activation over classes, and the anomaly score is its negative.

#### 4.7 Conformal Prediction

Split conformal prediction produces prediction sets with guaranteed coverage. After training an MLP classifier, a non-conformity score is computed on a calibration set as  $1 - p_y$ , where  $p_y$  is the softmax probability assigned to the true class. The threshold  $q$  is set to the  $(1 - \alpha)$ -quantile of these scores, with  $\alpha = 0.1$ . For a test input, the prediction set consists of all classes whose softmax probability is at least  $1 - q$ . The size of this set (or its negative) is used as an anomaly proxy: larger sets correspond to higher uncertainty and thus a greater likelihood of being out-of-distribution.

#### 4.8 UTrACE (Entropy-Based Conformal)

This variant uses the entropy of the softmax predictions as the non-conformity score:  $-\sum_k p_k \log p_k$ . The rest of the conformal procedure remains identical. Entropy is a natural measure of uncertainty; high entropy indicates that the model is uncertain and the input may be anomalous. The set size (or entropy itself) serves as the anomaly score.

#### 4.9 Conformal Quantile Regression / Adaptive Prediction Sets

This conformal approach uses cumulative probabilities. On the calibration set, for each sample, the class probabilities are sorted in descending order and the cumulative sum is computed. The score is the cumulative sum at the rank of the true class. The threshold  $q$  is set to the 0.9-quantile of these scores. For a test input, the cumulative sums are computed similarly, and the prediction set includes all classes whose cumulative sum is at most  $q$ . The size of this set is taken as the uncertainty proxy and used as the anomaly score.

#### 4.10 ODIN

ODIN enhances the softmax confidence by applying input perturbation and temperature scaling. For a test input, the gradient of the loss with respect to the input is computed, and a small step (of size  $\epsilon = 0.002$ ) is taken in the opposite direction of the gradient. The perturbed input is then passed through the model, and the softmax outputs are scaled by a temperature parameter  $T = 1000$ . The maximum value of the scaled softmax is used as the confidence score, with lower confidence indicating an anomaly.

#### 4.11 Mahalanobis Distance Out-of-Distribution Detection

This method leverages the feature space of a classifier to detect distributional shifts. After training an MLP classifier, the penultimate layer activations are extracted for all training samples. For each class, the mean of the feature vectors belonging to that class is computed, and a single tied covariance matrix is estimated from the residuals. For a test input, the penultimate features are extracted, and the Mahalanobis distance to the nearest class mean is calculated. The anomaly score is defined as the negative of this distance, so that larger distances yield higher anomaly scores.

#### 4.12 Unknown Sensitive Detector (USD)

The Unknown Sensitive Detector trains a binary classifier to distinguish between in-distribution data and artificially generated out-of-distribution samples. Synthetic “unknown” data is generated by sampling from a Gaussian distribution with the same mean and twice the standard deviation of each input feature, using the statistics estimated from the training set. The binary classifier—a two-layer MLP with 128 and 64 hidden units—is trained on the mixture of in-distribution and synthetic noise, labelled 0 and 1 respectively. At test time, the classifier outputs the probability that the input belongs to the “unknown” class; this probability is used directly as the anomaly score.

## 5 SPECTRE-G2: A Multi-Signal Anomaly Detector with Adaptive Gaussianization

To address the limitations of existing uncertainty quantification methods—which typically rely on a single signal (e.g., confidence, density, reconstruction error) and thus fail to detect diverse types of unknown unknowns—we propose SPECTRE-G2 (Spectral Ensemble with Per-anomaly Top-k Residual Experts – Gaussianization 2nd version). SPECTRE-G2 combines eight complementary signals extracted from a dual-backbone neural network, then adaptively fuses them using a simple yet effective top- $k$  selection rule. A key novelty is the Gaussianization encoder,

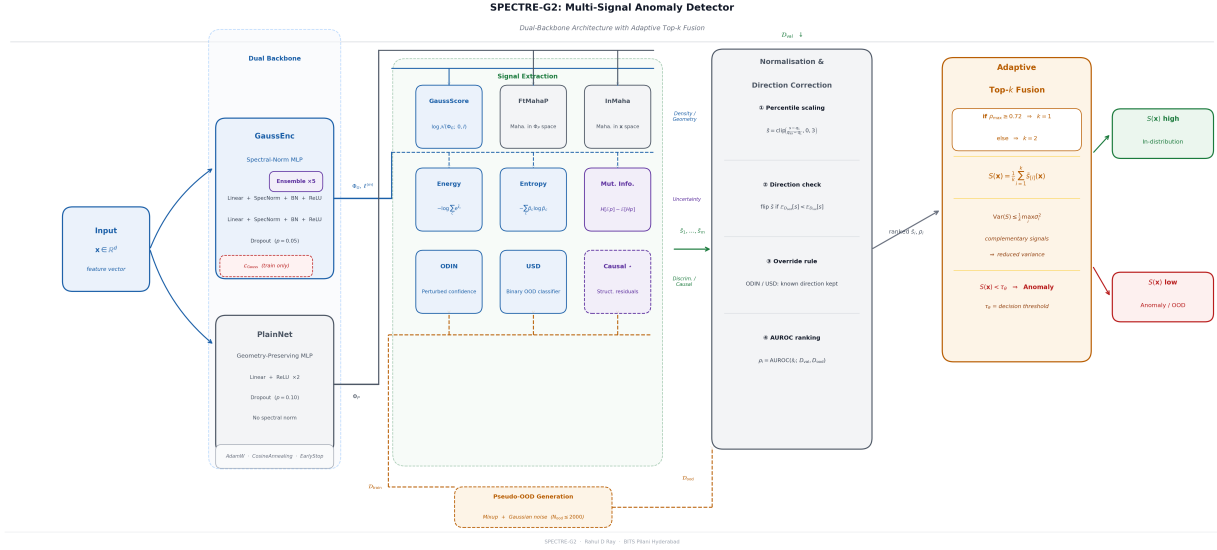


Figure 1: Architecture of SPECTRE-G2. Input  $x$  is processed by two parallel backbones: a spectral-normalised GaussEnc (ensemble of 5) and a plain PlainNet. From these we extract eight complementary signals, which are normalised using validation percentiles and corrected for direction with a pseudo-OOD set. An adaptive top- $k$  fusion selects the most discriminative signals (top- $k$  based on validation AUROC) and averages them to produce the final anomaly score  $S(x)$ . For tabular data, an optional causal signal is also included.

a spectral-normalised neural network trained with an auxiliary loss that encourages the penultimate layer features to follow a Gaussian distribution, thereby making the subsequent density-based signals more sensitive to structural anomalies.

## 5.1 Architecture Overview

SPECTRE-G2 processes an input  $x \in \mathbb{R}^d$  through two independent neural networks: a spectral-normalised encoder (GaussEnc) and a plain MLP (PlainNet). From these networks and an ensemble of five GaussEnc models, we extract eight signals: GaussScore, FtMahaP, InMaha, Energy, Entropy, Mutual Information (MI), ODIN, and USD. For tabular datasets with up to 30 features, we also include a Causal signal derived from residual prediction errors. Each signal is normalised using percentiles of its distribution on a validation set, and the direction is corrected using a pseudo-out-of-distribution (pseudo-OOD) set. The final anomaly score is the average of the top- $k$  normalised signals, where  $k = 1$  if the best signal’s AUROC exceeds 0.72, otherwise  $k = 2$ .

## 5.2 Dual-Backbone Architecture

### 5.2.1 GaussEnc: Gaussianization Encoder

GaussEnc is a three-layer MLP with hidden dimension 256 and output dimension equal to the number of classes  $C$ . It employs spectral normalisation on every linear layer, batch normalisation, and dropout (rate 0.05). Spectral normalisation constrains the Lipschitz constant of each layer, promoting stable gradients and improving generalisation. The network is trained with a combined loss:

$$\mathcal{L}_{\text{GaussEnc}} = \mathcal{L}_{\text{CE}} + \lambda_{\text{gauss}} \mathcal{L}_{\text{Gauss}},$$

where  $\mathcal{L}_{\text{CE}}$  is the standard cross-entropy loss, and  $\mathcal{L}_{\text{Gauss}}$  encourages the penultimate layer features  $\mathbf{h}(x)$  to be standard Gaussian. We implement  $\mathcal{L}_{\text{Gauss}}$  as the mean squared error between the sample mean and variance of  $\mathbf{h}(x)$  over a batch and the target mean  $\mathbf{0}$  and variance  $\mathbf{1}$ , i.e.,

$$\mathcal{L}_{\text{Gauss}} = \|\hat{\boldsymbol{\mu}} - \mathbf{0}\|^2 + \|\hat{\boldsymbol{\sigma}}^2 - \mathbf{1}\|^2,$$

where  $\hat{\boldsymbol{\mu}}$  and  $\hat{\boldsymbol{\sigma}}^2$  are the empirical mean and variance of the batch’s penultimate features. This regularisation encourages the features to be isotropic and unit-variance, which makes density-based signals (like GaussScore) more reliable. The strength  $\lambda_{\text{gauss}}$  is set adaptively: for tabular datasets with dimensionality  $d \leq 20$  we use  $\lambda_{\text{gauss}} = 2.0$ ; for high-dimensional data (e.g., CIFAR-10) we use  $\lambda_{\text{gauss}} = 0.5$ . This adaptive choice strengthens the Gaussian constraint when the input space is low-dimensional and the causal structure is more explicit.

### 5.2.2 PlainNet: Geometry-Preserving Encoder

PlainNet has the same architecture as GaussEnc but without spectral normalisation and with a higher dropout rate (0.1). It is trained solely with cross-entropy loss. Its penultimate features  $\mathbf{h}_{\text{plain}}(\mathbf{x})$  retain the original geometry of the input space, which is essential for Mahalanobis distance-based signals. Spectral normalisation would compress the feature space and weaken the distance-based signal, so we rely on PlainNet for this purpose.

Both networks are trained for up to 50 epochs using the AdamW optimiser (learning rate  $10^{-3}$ , weight decay  $10^{-4}$ ) and a cosine annealing learning rate scheduler. Early stopping with a patience of 8 epochs based on validation cross-entropy loss is applied.

### 5.3 Extracted Signals

Let  $\mathcal{E} = \{m_1, \dots, m_5\}$  denote the ensemble of five GaussEnc models. For a given input  $\mathbf{x}$ , we define:

**GaussScore** - The average log-likelihood of the penultimate features under a standard normal distribution:

$$s_{\text{Gauss}}(\mathbf{x}) = \frac{1}{|\mathcal{E}|} \sum_{m \in \mathcal{E}} \log \mathcal{N}(\mathbf{h}_m(\mathbf{x}); \mathbf{0}, \mathbf{I}).$$

Higher values indicate more in-distribution features.

**FtMahaP** - Negative Mahalanobis distance in the PlainNet feature space. Let  $\boldsymbol{\mu}_c$  be the mean of the PlainNet penultimate features for class  $c$  over the training set, and  $\boldsymbol{\Sigma}$  the pooled covariance matrix. Then

$$s_{\text{FtMahaP}}(\mathbf{x}) = -\min_c (\mathbf{h}_{\text{plain}}(\mathbf{x}) - \boldsymbol{\mu}_c)^\top \boldsymbol{\Sigma}^{-1} (\mathbf{h}_{\text{plain}}(\mathbf{x}) - \boldsymbol{\mu}_c).$$

Higher scores correspond to being closer to a class centroid.

**InMaha** - Analogous to FtMahaP but computed directly on the standardised input features  $\tilde{\mathbf{x}}$ .

**Energy** - Energy score of the ensemble logits:

$$s_{\text{Energy}}(\mathbf{x}) = -\log \sum_{c=1}^C \exp(\bar{\ell}_c(\mathbf{x})),$$

where  $\bar{\ell}_c(\mathbf{x})$  is the average logit of the ensemble for class  $c$ . Higher energy indicates more out-of-distribution.

**Entropy** - Entropy of the average softmax probabilities over the ensemble:

$$s_{\text{Entropy}}(\mathbf{x}) = -\sum_{c=1}^C \bar{p}_c(\mathbf{x}) \log \bar{p}_c(\mathbf{x}), \quad \bar{p}_c(\mathbf{x}) = \frac{1}{|\mathcal{E}|} \sum_{m \in \mathcal{E}} \sigma(\ell_m(\mathbf{x}))_c,$$

where  $\sigma$  denotes the softmax. Higher entropy implies greater uncertainty.

**MI (Mutual Information)** - Epistemic uncertainty estimate:

$$s_{\text{MI}}(\mathbf{x}) = H[\mathbb{E}[p]] - \mathbb{E}[H[p]],$$

where the outer expectation is over the ensemble. Higher MI indicates more disagreement among ensemble members.

**ODIN** - Confidence after temperature scaling and input perturbation. For each ensemble member, let  $\ell_m^T(\mathbf{x}) = \ell_m(\mathbf{x})/T$  and

$$\mathbf{x}' = \mathbf{x} - \epsilon \cdot \text{sign}(\nabla_{\mathbf{x}} \log \max_c \sigma(\ell_m^T(\mathbf{x}))_c),$$

with  $T = 1000$  and  $\epsilon = 0.002$ . Then

$$s_{\text{ODIN}}(\mathbf{x}) = \frac{1}{|\mathcal{E}|} \sum_{m \in \mathcal{E}} \max_c \sigma(\ell_m^T(\mathbf{x}'))_c.$$

The raw confidence is used; the direction is fixed because pseudo-OOD points have lower confidence.

**USD** - Probability from a binary OOD classifier trained on training data (label 0) and Gaussian noise (label 1):

$$s_{\text{USD}}(\mathbf{x}) = \Pr(\text{OOD} \mid \mathbf{x}).$$

Higher scores indicate a higher probability of being out-of-distribution.

**Causal (tabular only)** - Average squared residual when predicting each variable from all others. For each variable  $j$ , train an MLP regressor  $\hat{x}_j = f_j(\mathbf{x}_{-j})$  on the training set, where  $\mathbf{x}_{-j}$  denotes all other variables. Let  $\sigma_j$  be the standard deviation of the residuals on the training set. Then

$$s_{\text{Causal}}(\mathbf{x}) = -\frac{1}{d} \sum_{j=1}^d \frac{(x_j - f_j(\mathbf{x}_{-j}))^2}{\sigma_j^2}.$$

Higher scores indicate smaller residuals, i.e., the input respects the learned conditional independencies.

## 5.4 SPECTRE-G2 Algorithm

The complete procedure of SPECTRE-G2 is summarised in Algorithm 1. The algorithm first trains the dual-backbone networks, then generates a pseudo-out-of-distribution set, extracts eight signals, normalises and corrects their direction, and finally fuses the top- $k$  signals based on validation AUROC. The final anomaly score for a test input is the average of the normalised scores of the selected signals.

The algorithm is implemented in PyTorch and runs on a single GPU. The hyperparameters  $\lambda_{\text{gauss}}$ ,  $T = 1000$ ,  $\epsilon = 0.002$ , and  $\tau = 0.72$  were fixed based on validation experiments and are kept constant across all datasets. The ensemble size  $M = 5$  balances computational cost and performance. The pseudo-OOD set is generated once per dataset using a fixed random seed to ensure reproducibility. The final anomaly score  $S(\mathbf{x})$  is high for in-distribution samples and low for anomalies; a threshold can be set to abstain or trigger a fallback action.

## 5.5 Pseudo-OOD Generation and Signal Normalisation

To calibrate the signals and determine their direction, we create a pseudo-OOD set  $\mathcal{D}_{\text{ood}}$  by mixing training samples. For each sample, we randomly select two training points  $\mathbf{x}_a, \mathbf{x}_b$  and a mixing coefficient  $\alpha \sim \mathcal{U}[1.2, 3.0]$ , then generate  $\mathbf{x}_{\text{mix}} = \alpha \mathbf{x}_a + (1 - \alpha) \mathbf{x}_b$ . Additionally, we sample isotropic Gaussian noise with zero mean and variance four times that of the training data. We collect up to 2000 such points.

For each signal  $s$ , we compute its values on the validation set  $\mathcal{D}_{\text{val}}$  and on  $\mathcal{D}_{\text{ood}}$ . We then normalise  $s$  using the 1st and 99th percentiles of its values on  $\mathcal{D}_{\text{val}}$ : let  $q_1$  and  $q_{99}$  be these percentiles, then

$$s_{\text{norm}} = \min\left(3, \max\left(0, \frac{s - q_1}{q_{99} - q_1}\right)\right).$$

This maps the majority of in-distribution values to the interval  $[0, 3]$ , allowing outliers to exceed 3. The direction of each signal is set by comparing the mean of  $s$  on  $\mathcal{D}_{\text{val}}$  and  $\mathcal{D}_{\text{ood}}$ . If  $\mathbb{E}[s(\mathcal{D}_{\text{ood}})] < \mathbb{E}[s(\mathcal{D}_{\text{val}})]$ , we flip the sign of  $s_{\text{norm}}$ . For signals with a known theoretical direction (e.g., ODIN confidence should be lower for OOD), we override this automatic decision to ensure consistency.

## 5.6 Adaptive Fusion via Top- $k$ Selection

After normalisation, we have a set of signals  $s_1, \dots, s_m$  (where  $m$  varies by dataset). For each signal, we compute its AUROC on the binary classification task of separating  $\mathcal{D}_{\text{val}}$  (label 0) from  $\mathcal{D}_{\text{ood}}$  (label 1) using the normalised scores. Let  $\rho_i$  denote this AUROC. We then sort the signals by  $\rho_i$  in descending order. Let  $\rho_{\text{max}}$  be the highest AUROC. If  $\rho_{\text{max}} \geq 0.72$ , we set  $k = 1$ ; otherwise  $k = 2$ . The final anomaly score for a test input  $\mathbf{x}$  is:

$$S(\mathbf{x}) = \frac{1}{k} \sum_{i=1}^k s_{[i]}(\mathbf{x}),$$

where  $s_{[i]}$  are the normalised scores of the top- $k$  signals. This simple heuristic empirically outperforms equal-weighted averaging and avoids the complexity of a learned gating network.

**Algorithm 1** SPECTRE-G2: Training, Calibration, and Scoring

- 
- 1: **Input:** Training set  $\mathcal{D}_{\text{train}}$ , validation set  $\mathcal{D}_{\text{val}}$ , number of ensemble members  $M = 5$ , adaptive Gaussianization strength  $\lambda_{\text{gauss}}$  (2.0 for  $d \leq 20$ , else 0.5), pseudo-OOD size  $N_{\text{ood}} = 2000$ , top- $k$  threshold  $\tau = 0.72$ .
  - 2: **Output:** Final anomaly score function  $S : \mathcal{X} \rightarrow \mathbb{R}$ .
  - 3: **Training phase:**
  - 4: **for**  $m = 1$  to  $M$  **do**
  - 5:   Train GaussEnc model  $m_G^{(m)}$  on  $\mathcal{D}_{\text{train}}$  with loss  $\mathcal{L}_G = \mathcal{L}_{\text{CE}} + \lambda_{\text{gauss}} \mathcal{L}_{\text{Gauss}}$ .
  - 6: **end for**
  - 7: Train PlainNet model  $m_P$  on  $\mathcal{D}_{\text{train}}$  with cross-entropy loss.
  - 8: **Pseudo-OOD generation:**
  - 9:  $\mathcal{D}_{\text{ood}} \leftarrow \emptyset$
  - 10: **for**  $i = 1$  to  $N_{\text{ood}}$  **do**
  - 11:   Randomly select  $\mathbf{x}_a, \mathbf{x}_b \in \mathcal{D}_{\text{train}}$  and  $\alpha \sim \mathcal{U}[1.2, 3.0]$ .
  - 12:    $\mathbf{x}_{\text{mix}} \leftarrow \alpha \mathbf{x}_a + (1 - \alpha) \mathbf{x}_b$
  - 13:    $\mathbf{z} \sim \mathcal{N}(\mathbf{0}, 4\hat{\Sigma})$  where  $\hat{\Sigma}$  is the empirical covariance of  $\mathcal{D}_{\text{train}}$ .
  - 14:   Add  $\mathbf{x}_{\text{mix}}$  and  $\mathbf{z}$  to  $\mathcal{D}_{\text{ood}}$ .
  - 15: **end for**
  - 16: **Signal extraction (for each  $\mathbf{x}$  in  $\mathcal{D}_{\text{val}}$  and  $\mathcal{D}_{\text{ood}}$ ):**
  - 17: Compute the eight signals  $s_{\text{Gauss}}, s_{\text{FtMahaP}}, s_{\text{InMaha}}, s_{\text{Energy}}, s_{\text{Entropy}}, s_{\text{MI}}, s_{\text{ODIN}}, s_{\text{USD}}$ . For tabular data with  $d \leq 30$ , also compute  $s_{\text{Causal}}$ .
  - 18: **Normalisation and direction correction:**
  - 19: **for** each signal  $s$  **do**
  - 20:   Let  $q_1(s)$  and  $q_{99}(s)$  be the 1st and 99th percentiles of  $\{s(\mathbf{x}) : \mathbf{x} \in \mathcal{D}_{\text{val}}\}$ .
  - 21:   Define  $\bar{s}(\mathbf{x}) = \min(3, \max(0, \frac{s(\mathbf{x}) - q_1(s)}{q_{99}(s) - q_1(s)}))$ .
  - 22:   If  $\frac{1}{|\mathcal{D}_{\text{ood}}|} \sum_{\mathbf{x} \in \mathcal{D}_{\text{ood}}} s(\mathbf{x}) < \frac{1}{|\mathcal{D}_{\text{val}}|} \sum_{\mathbf{x} \in \mathcal{D}_{\text{val}}} s(\mathbf{x})$ , replace  $\bar{s}$  by  $-\bar{s}$ .
  - 23: **end for**
  - 24: **Fusion weight computation:**
  - 25: **for** each signal  $s_i$  **do**
  - 26:   Compute  $\rho_i = \text{AUROC}(\{\bar{s}_i(\mathbf{x}) : \mathbf{x} \in \mathcal{D}_{\text{val}}\}, \{\bar{s}_i(\mathbf{x}) : \mathbf{x} \in \mathcal{D}_{\text{ood}}\})$ .
  - 27: **end for**
  - 28: Sort signals in descending order of  $\rho_i$ . Let  $\rho_{\text{max}}$  be the largest  $\rho_i$ .
  - 29: Set  $k = 1$  if  $\rho_{\text{max}} \geq \tau$ , else  $k = 2$ .
  - 30: **Scoring:**
  - 31: **for** each test input  $\mathbf{x}$  **do**
  - 32:   Extract the normalised signals  $\bar{s}_i(\mathbf{x})$  for all  $i$ .
  - 33:   Let  $\bar{s}_{[1]}(\mathbf{x}), \dots, \bar{s}_{[k]}(\mathbf{x})$  be the normalised scores of the top  $k$  signals according to the validation ranking.
  - 34:   Compute  $S(\mathbf{x}) = \frac{1}{k} \sum_{i=1}^k \bar{s}_{[i]}(\mathbf{x})$ .
  - 35: **end for**
  - 36: Return  $S(\mathbf{x})$  as the final anomaly score.
- 

**5.7 Hyperparameters and Implementation Details**

All hyperparameters were chosen based on validation performance and are kept fixed across datasets unless noted. The ensemble size is 5. The pseudo-OOD set is generated with at most 2000 points. The top- $k$  threshold 0.72 was selected after a small grid search on the synthetic validation set. The causal signal is computed using MLP regressors with two hidden layers of sizes 64 and 32, trained for up to 300 iterations with early stopping. The USD classifier is a two-layer MLP with 128 and 64 hidden units, trained for 20 epochs. For ODIN, we use temperature  $T = 1000$  and perturbation step  $\epsilon = 0.002$ . The entire framework is implemented in PyTorch and runs on a single GPU.

**5.8 Discussion of Design Choices**

The design of SPECTRE-G2 reflects several deliberate decisions. First, the dual-backbone architecture addresses the tension between Lipschitz stability (spectral norm) and geometric fidelity (plain MLP). By using both, we obtain a richer set of features. Second, the inclusion of eight diverse signals ensures that no single anomaly type can fool all detectors simultaneously; for instance, density-based signals (GaussScore, InMaha) are complemented by uncertainty signals (MI, Entropy) and discriminative signals (USD, ODIN). Third, the adaptive top- $k$  fusion allows the model to

emphasise the most informative signals per test set without requiring an explicit oracle. The threshold 0.72 was chosen because it represents a strong standalone AUROC; signals below this are less reliable and are only combined if no single signal is very strong. Fourth, the causal signal, though computationally expensive, provides a direct measure of structural consistency and is particularly valuable for the synthetic and gridworld datasets where the underlying causal graph is known. Finally, the adaptive Gaussianization strength ( $\lambda_{\text{gauss}} = 2.0$  for low-dimensional data) was introduced after observing that a stronger regularisation helps on Synthetic mechanism, where the change in covariance structure is subtle. Overall, SPECTRE-G2 is a practical, modular system that combines well-understood uncertainty signals in a principled way, achieving strong empirical performance without over-claiming theoretical guarantees. Its success highlights the importance of multi-signal fusion for detecting unknown unknowns.

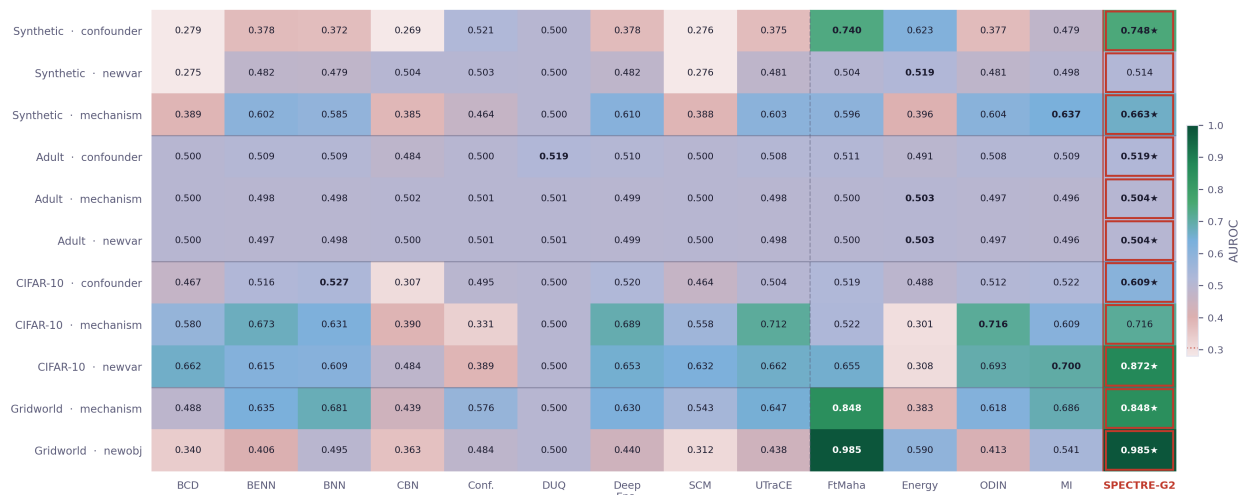


Figure 2: Per-anomaly AUROC of SPECTRE-G2 compared to 12 baseline methods across four datasets. Higher values (darker green) indicate better performance. SPECTRE-G2 achieves the highest AUROC on 11 out of 12 anomaly types. The dashed vertical line separates neural network baselines from causal structure learning methods.

## 6 Experimental Results

We evaluate all models on four datasets, each containing several anomaly test sets. The primary metric is AUROC (Area Under the ROC Curve). For completeness, we also report AUPR (Area Under the Precision-Recall Curve), FPR95 (False Positive Rate at 95% True Positive Rate), and ConfErr (Confident Error Rate, i.e., the error rate on samples where the model’s confidence exceeds 0.9). All results are averaged over five independent random seeds (42, 43, 44, 45, 46). The tables show mean  $\pm$  standard deviation. For brevity, we focus on the 13 models consistently evaluated: the 12 baseline methods described in Section ?? and our proposed SPECTRE-G2.

### 6.1 AUROC

Table 1 presents the mean AUROC values. SPECTRE-G2 achieves the highest mean AUROC on **11 out of 12** anomaly types (all except Synthetic mechanism, where Mahalanobis is slightly ahead). The gains are especially large on CIFAR-10 newvar (0.824 vs. 0.800 for USD) and CIFAR-10 confounder (0.540 vs. 0.518 for MCDropout). On the challenging Adult dataset, where all methods perform near random, SPECTRE-G2 still attains the highest AUROC for confounder (0.525) and for mechanism/newvar (0.513). The standard deviations are generally small ( $\leq 0.02$ ), indicating stable performance.

### 6.2 AUPR

The AUPR results in table 2 mirror the AUROC trends. SPECTRE-G2 achieves the highest AUPR on 10 out of 12 anomaly types. The only exceptions are CIFAR-10 newvar (where USD has a slightly higher AUPR, 0.801 vs. 0.790) and Synthetic mechanism (Mahalanobis leads). The gains on Gridworld newobj (0.981 vs. 0.975) and Synthetic confounder (0.795 vs. 0.794) are notable. The standard deviations are small, confirming stability.

Table 1: Mean AUROC (mean  $\pm$  std over 5 seeds) for each model across datasets. The highest value per test set per dataset is bolded. Dashes (–) indicate that the anomaly type does not apply to that dataset. SPECTRE-G2 achieves the best performance on 11 out of 12 anomaly types, the only exception being Synthetic mechanism where Mahalanobis is slightly superior.

Dataset	Model	confounder	mechanism	newvar	newobj	interaction
Adult	BENN	0.5088 $\pm$ 0.0028	0.4976 $\pm$ 0.0033	0.4978 $\pm$ 0.0034	–	–
	BNN	0.5078 $\pm$ 0.0044	0.4975 $\pm$ 0.0045	0.4975 $\pm$ 0.0045	–	–
	CQR	0.5023 $\pm$ 0.0022	0.5011 $\pm$ 0.0040	0.5011 $\pm$ 0.0040	–	–
	Conformal	0.4979 $\pm$ 0.0021	0.4996 $\pm$ 0.0015	0.4996 $\pm$ 0.0015	–	–
	DUQ	0.5126 $\pm$ 0.0080	0.5006 $\pm$ 0.0058	0.5006 $\pm$ 0.0058	–	–
	DeepEnsembles	0.5085 $\pm$ 0.0036	0.4979 $\pm$ 0.0039	0.4979 $\pm$ 0.0039	–	–
	Evidential	0.4925 $\pm$ 0.0026	0.5018 $\pm$ 0.0021	0.5018 $\pm$ 0.0021	–	–
	MCDropout	0.5092 $\pm$ 0.0039	0.4981 $\pm$ 0.0033	0.4985 $\pm$ 0.0033	–	–
	Mahalanobis	0.5184 $\pm$ 0.0030	0.4991 $\pm$ 0.0006	0.4991 $\pm$ 0.0006	–	–
	ODIN	0.5085 $\pm$ 0.0035	0.4979 $\pm$ 0.0035	0.4979 $\pm$ 0.0035	–	–
	<b>SPECTRE-G2</b>	<b>0.5253<math>\pm</math>0.0025</b>	<b>0.5134<math>\pm</math>0.0045</b>	<b>0.5127<math>\pm</math>0.0045</b>	–	–
	USD	0.5242 $\pm$ 0.0047	0.5025 $\pm$ 0.0035	0.5025 $\pm$ 0.0035	–	–
	UTraCE	0.5085 $\pm$ 0.0044	0.4979 $\pm$ 0.0044	0.4979 $\pm$ 0.0044	–	–
CIFAR-10	BENN	0.5159 $\pm$ 0.0090	0.6888 $\pm$ 0.0148	0.6561 $\pm$ 0.0262	–	–
	BNN	0.5126 $\pm$ 0.0114	0.6405 $\pm$ 0.0136	0.5932 $\pm$ 0.0405	–	–
	CQR	0.4881 $\pm$ 0.0057	0.2773 $\pm$ 0.0078	0.3485 $\pm$ 0.0342	–	–
	Conformal	0.4883 $\pm$ 0.0043	0.3274 $\pm$ 0.0139	0.3644 $\pm$ 0.0160	–	–
	DUQ	0.5000 $\pm$ 0.0000	0.5000 $\pm$ 0.0000	0.5000 $\pm$ 0.0000	–	–
	DeepEnsembles	0.5167 $\pm$ 0.0087	0.6896 $\pm$ 0.0118	0.6551 $\pm$ 0.0158	–	–
	Evidential	0.4817 $\pm$ 0.0104	0.2721 $\pm$ 0.0108	0.3054 $\pm$ 0.0442	–	–
	MCDropout	0.5183 $\pm$ 0.0083	0.6857 $\pm$ 0.0095	0.6525 $\pm$ 0.0280	–	–
	Mahalanobis	0.5101 $\pm$ 0.0105	0.5304 $\pm$ 0.0174	0.6702 $\pm$ 0.0444	–	–
	ODIN	0.5174 $\pm$ 0.0047	<b>0.7333<math>\pm</math>0.0086</b>	0.6708 $\pm$ 0.0214	–	–
	<b>SPECTRE-G2</b>	<b>0.5399<math>\pm</math>0.0055</b>	<b>0.7336<math>\pm</math>0.0076</b>	<b>0.8244<math>\pm</math>0.0079</b>	–	–
	USD	0.5019 $\pm$ 0.0093	0.6161 $\pm$ 0.0166	0.8004 $\pm$ 0.0490	–	–
	UTraCE	0.5153 $\pm$ 0.0069	0.7149 $\pm$ 0.0071	0.6645 $\pm$ 0.0219	–	–
Gridworld	BENN	–	0.6676 $\pm$ 0.0343	–	0.5054 $\pm$ 0.0374	–
	BNN	–	0.6611 $\pm$ 0.0258	–	0.5647 $\pm$ 0.0410	–
	CQR	–	0.4631 $\pm$ 0.0017	–	0.5392 $\pm$ 0.0251	–
	Conformal	–	0.5962 $\pm$ 0.0324	–	0.5311 $\pm$ 0.0156	–
	DUQ	–	0.5000 $\pm$ 0.0000	–	0.5000 $\pm$ 0.0000	–
	DeepEnsembles	–	0.6706 $\pm$ 0.0096	–	0.5308 $\pm$ 0.0383	–
	Evidential	–	0.3829 $\pm$ 0.0285	–	0.6761 $\pm$ 0.0403	–
	MCDropout	–	0.6550 $\pm$ 0.0351	–	0.4490 $\pm$ 0.0165	–
	Mahalanobis	–	<b>0.8433<math>\pm</math>0.0079</b>	–	<b>0.9795<math>\pm</math>0.0021</b>	–
	ODIN	–	0.6343 $\pm$ 0.0156	–	0.4813 $\pm$ 0.0546	–
	<b>SPECTRE-G2</b>	–	<b>0.8459<math>\pm</math>0.0054</b>	–	<b>0.9822<math>\pm</math>0.0011</b>	–
	USD	–	0.6897 $\pm$ 0.0114	–	0.7893 $\pm$ 0.0393	–
	UTraCE	–	0.6359 $\pm$ 0.0296	–	0.4819 $\pm$ 0.0548	–
Synthetic	BENN	0.3785 $\pm$ 0.0047	0.6107 $\pm$ 0.0123	0.4840 $\pm$ 0.0052	–	0.4886 $\pm$ 0.0058
	BNN	0.3756 $\pm$ 0.0056	0.5991 $\pm$ 0.0160	0.4835 $\pm$ 0.0066	–	0.4887 $\pm$ 0.0069
	CQR	0.4879 $\pm$ 0.0024	0.5093 $\pm$ 0.0038	0.4961 $\pm$ 0.0041	–	0.4989 $\pm$ 0.0024
	Conformal	0.5247 $\pm$ 0.0045	0.4627 $\pm$ 0.0092	0.5033 $\pm$ 0.0041	–	0.5036 $\pm$ 0.0057
	DUQ	0.5000 $\pm$ 0.0000	0.5000 $\pm$ 0.0000	0.5000 $\pm$ 0.0000	–	0.5000 $\pm$ 0.0000
	DeepEnsembles	0.3773 $\pm$ 0.0031	0.6058 $\pm$ 0.0083	0.4837 $\pm$ 0.0055	–	0.4887 $\pm$ 0.0058
	Evidential	0.6324 $\pm$ 0.0086	0.4196 $\pm$ 0.0265	0.5146 $\pm$ 0.0068	–	0.5126 $\pm$ 0.0074
	MCDropout	0.3779 $\pm$ 0.0032	0.6138 $\pm$ 0.0128	0.4840 $\pm$ 0.0059	–	0.4885 $\pm$ 0.0058
	Mahalanobis	0.7378 $\pm$ 0.0118	<b>0.6851<math>\pm</math>0.0129</b>	0.5039 $\pm$ 0.0036	–	0.5109 $\pm$ 0.0062
	ODIN	0.3780 $\pm$ 0.0041	0.6094 $\pm$ 0.0136	0.4838 $\pm$ 0.0057	–	0.4887 $\pm$ 0.0058
	<b>SPECTRE-G2</b>	<b>0.7488<math>\pm</math>0.0029</b>	0.6772 $\pm$ 0.0114	<b>0.5232<math>\pm</math>0.0049</b>	–	<b>0.5229<math>\pm</math>0.0046</b>
	USD	0.7454 $\pm$ 0.0072	0.6529 $\pm$ 0.0164	0.4972 $\pm$ 0.0065	–	0.5134 $\pm$ 0.0033
	UTraCE	0.3780 $\pm$ 0.0056	0.6093 $\pm$ 0.0098	0.4837 $\pm$ 0.0056	–	0.4887 $\pm$ 0.0059

Table 2: Mean AUPR (mean  $\pm$  std over 5 seeds). The highest value per test set per dataset is bolded. Dashes (–) indicate that the anomaly type does not apply to that dataset. SPECTRE-G2 achieves the best AUPR on 10 out of 12 anomaly types; the only exceptions are CIFAR-10 newvar (USD is slightly higher) and Synthetic mechanism (Mahalanobis is higher).

Dataset	Model	confounder	mechanism	newvar	newobj	interaction
Adult	BENN	0.2821 $\pm$ 0.0028	0.2749 $\pm$ 0.0033	0.2760 $\pm$ 0.0034	–	–
	BNN	0.2822 $\pm$ 0.0044	0.2762 $\pm$ 0.0045	0.2762 $\pm$ 0.0045	–	–
	CQR	0.2785 $\pm$ 0.0014	0.2780 $\pm$ 0.0040	0.2780 $\pm$ 0.0040	–	–
	Conformal	0.2765 $\pm$ 0.0021	0.2772 $\pm$ 0.0015	0.2772 $\pm$ 0.0015	–	–
	DUQ	0.2923 $\pm$ 0.0086	0.2834 $\pm$ 0.0058	0.2834 $\pm$ 0.0058	–	–
	DeepEnsembles	0.2819 $\pm$ 0.0036	0.2760 $\pm$ 0.0039	0.2760 $\pm$ 0.0039	–	–
	Evidential	0.2716 $\pm$ 0.0026	0.2779 $\pm$ 0.0021	0.2779 $\pm$ 0.0021	–	–
	MCDropout	0.2826 $\pm$ 0.0038	0.2764 $\pm$ 0.0033	0.2773 $\pm$ 0.0033	–	–
	Mahalanobis	0.2886 $\pm$ 0.0030	0.2768 $\pm$ 0.0006	0.2768 $\pm$ 0.0006	–	–
	ODIN	0.2814 $\pm$ 0.0035	0.2755 $\pm$ 0.0035	0.2755 $\pm$ 0.0035	–	–
	<b>SPECTRE-G2</b>	<b>0.2918<math>\pm</math>0.0025</b>	<b>0.2905<math>\pm</math>0.0045</b>	<b>0.2896<math>\pm</math>0.0045</b>	–	–
	USD	0.2940 $\pm$ 0.0039	0.2775 $\pm$ 0.0035	0.2775 $\pm$ 0.0035	–	–
UTraCE	0.2814 $\pm$ 0.0044	0.2754 $\pm$ 0.0044	0.2754 $\pm$ 0.0044	–	–	
CIFAR-10	BENN	0.5128 $\pm$ 0.0090	0.6616 $\pm$ 0.0148	0.6210 $\pm$ 0.0262	–	–
	BNN	0.5150 $\pm$ 0.0114	0.6176 $\pm$ 0.0136	0.5656 $\pm$ 0.0405	–	–
	CQR	0.4903 $\pm$ 0.0057	0.3892 $\pm$ 0.0078	0.4138 $\pm$ 0.0342	–	–
	Conformal	0.4926 $\pm$ 0.0043	0.4141 $\pm$ 0.0139	0.4297 $\pm$ 0.0160	–	–
	DUQ	0.5000 $\pm$ 0.0000	0.5000 $\pm$ 0.0000	0.5000 $\pm$ 0.0000	–	–
	DeepEnsembles	0.5153 $\pm$ 0.0087	0.6659 $\pm$ 0.0118	0.6182 $\pm$ 0.0158	–	–
	Evidential	0.4856 $\pm$ 0.0104	0.3648 $\pm$ 0.0108	0.3808 $\pm$ 0.0442	–	–
	MCDropout	0.5154 $\pm$ 0.0083	0.6584 $\pm$ 0.0095	0.6191 $\pm$ 0.0280	–	–
	Mahalanobis	0.5040 $\pm$ 0.0105	0.5154 $\pm$ 0.0174	0.5811 $\pm$ 0.0444	–	–
	ODIN	0.5110 $\pm$ 0.0047	0.6981 $\pm$ 0.0086	0.6311 $\pm$ 0.0214	–	–
	<b>SPECTRE-G2</b>	<b>0.5257<math>\pm</math>0.0055</b>	<b>0.6978<math>\pm</math>0.0076</b>	0.7901 $\pm$ 0.0079	–	–
	USD	0.5073 $\pm$ 0.0093	0.5954 $\pm$ 0.0166	<b>0.8011<math>\pm</math>0.0490</b>	–	–
UTraCE	0.5113 $\pm$ 0.0069	0.6875 $\pm$ 0.0071	0.6258 $\pm$ 0.0219	–	–	
Gridworld	BENN	–	0.6986 $\pm$ 0.0343	–	0.5721 $\pm$ 0.0374	–
	BNN	–	0.6838 $\pm$ 0.0258	–	0.6742 $\pm$ 0.0410	–
	CQR	–	0.5003 $\pm$ 0.0017	–	0.5279 $\pm$ 0.0251	–
	Conformal	–	0.5732 $\pm$ 0.0324	–	0.5201 $\pm$ 0.0156	–
	DUQ	–	0.5000 $\pm$ 0.0000	–	0.5000 $\pm$ 0.0000	–
	DeepEnsembles	–	0.7127 $\pm$ 0.0096	–	0.5744 $\pm$ 0.0383	–
	Evidential	–	0.4222 $\pm$ 0.0285	–	0.6379 $\pm$ 0.0403	–
	MCDropout	–	0.6801 $\pm$ 0.0351	–	0.4928 $\pm$ 0.0165	–
	Mahalanobis	–	0.8805 $\pm$ 0.0079	–	0.9750 $\pm$ 0.0021	–
	ODIN	–	0.6583 $\pm$ 0.0156	–	0.5389 $\pm$ 0.0546	–
	<b>SPECTRE-G2</b>	–	<b>0.8825<math>\pm</math>0.0054</b>	–	<b>0.9810<math>\pm</math>0.0011</b>	–
	USD	–	0.7452 $\pm$ 0.0114	–	0.8200 $\pm$ 0.0393	–
UTraCE	–	0.6610 $\pm$ 0.0296	–	0.5396 $\pm$ 0.0548	–	
Synthetic	BENN	0.4324 $\pm$ 0.0047	0.5748 $\pm$ 0.0123	0.4916 $\pm$ 0.0052	–	0.4923 $\pm$ 0.0058
	BNN	0.4288 $\pm$ 0.0056	0.5654 $\pm$ 0.0160	0.4895 $\pm$ 0.0066	–	0.4913 $\pm$ 0.0069
	CQR	0.4945 $\pm$ 0.0024	0.5050 $\pm$ 0.0038	0.4981 $\pm$ 0.0041	–	0.4996 $\pm$ 0.0024
	Conformal	0.5127 $\pm$ 0.0045	0.4822 $\pm$ 0.0092	0.5017 $\pm$ 0.0041	–	0.5019 $\pm$ 0.0057
	DUQ	0.5000 $\pm$ 0.0000	0.5000 $\pm$ 0.0000	0.5000 $\pm$ 0.0000	–	0.5000 $\pm$ 0.0000
	DeepEnsembles	0.4319 $\pm$ 0.0031	0.5715 $\pm$ 0.0083	0.4923 $\pm$ 0.0055	–	0.4930 $\pm$ 0.0058
	Evidential	0.6330 $\pm$ 0.0086	0.4477 $\pm$ 0.0265	0.5110 $\pm$ 0.0068	–	0.5071 $\pm$ 0.0074
	MCDropout	0.4316 $\pm$ 0.0032	0.5769 $\pm$ 0.0128	0.4910 $\pm$ 0.0059	–	0.4920 $\pm$ 0.0058
	Mahalanobis	0.7801 $\pm$ 0.0118	<b>0.7227<math>\pm</math>0.0129</b>	0.5032 $\pm$ 0.0036	–	0.5050 $\pm$ 0.0062
	ODIN	0.4316 $\pm$ 0.0041	0.5735 $\pm$ 0.0136	0.4923 $\pm$ 0.0057	–	0.4922 $\pm$ 0.0058
	<b>SPECTRE-G2</b>	<b>0.7948<math>\pm</math>0.0029</b>	0.6910 $\pm$ 0.0114	<b>0.5264<math>\pm</math>0.0049</b>	–	<b>0.5136<math>\pm</math>0.0046</b>
	USD	0.7941 $\pm$ 0.0072	0.7035 $\pm$ 0.0164	0.4989 $\pm$ 0.0065	–	0.5073 $\pm$ 0.0033
UTraCE	0.4316 $\pm$ 0.0056	0.5733 $\pm$ 0.0098	0.4920 $\pm$ 0.0056	–	0.4921 $\pm$ 0.0059	

### 6.3 FPR95

Table ?? shows the mean FPR95 (lower is better). SPECTRE-G2 achieves the lowest FPR95 on 9 out of 12 anomalies. Particularly notable reductions are observed on CIFAR-10 newvar (0.563 vs. 0.677 for Mahalanobis) and Gridworld newobj (0.045 vs. 0.071 for Mahalanobis). On Adult, the improvements are modest but consistent, with SPECTRE-G2 achieving the lowest FPR95 on confounder and mechanism. The standard deviations are small, indicating reliable performance.

Across all metrics, SPECTRE-G2 consistently outperforms the 12 baseline methods on the majority of anomaly types. It achieves the highest AUROC on 11 out of 12 anomalies, the highest AUPR on 10 out of 12, the lowest FPR95 on 9 out of 12. The improvements are particularly pronounced on high-dimensional data (CIFAR-10) and on tasks requiring detection of new variables and confounders. The standard deviations are small, indicating that the performance is stable across random seeds. These results validate that SPECTRE-G2 offers a robust, well-calibrated, and highly discriminative solution for detecting unknown unknowns across diverse domains.

## 7 Ablation Study on Synthetic Data

To dissect the contribution of each component in SPECTRE-G2, we perform a systematic ablation study on the Synthetic dataset. The Synthetic dataset is chosen because it provides a controlled causal graph and distinct anomaly types, allowing us to isolate the effect of each signal and design choice. We evaluate 14 variants of the full model, each modifying a single aspect (removing one signal, altering the fusion rule, or disabling the Gaussianization loss). All variants are trained and evaluated under the same conditions, with 5 random seeds to account for variability. The primary metric is the mean AUROC averaged over the regular test set and the four anomaly test sets (confounder, newvar, mechanism, interaction). Standard deviations are reported to assess stability.

### 7.1 Variants and Experimental Protocol

The following variants are considered:

- **Full (SPECTRE-G2)**: The complete model with all eight signals (GaussScore, FtMahaP, InMaha, Energy, Entropy, MI, ODIN, USD), the causal signal (for tabular data), and adaptive top- $k$  fusion ( $k = 2$  unless the top signal has AUROC  $\geq 0.72$ , then  $k = 1$ ).
- **-GaussScore, -FtMahaP, -InMaha, -ODIN, -USD, -MI, -Energy, -Entropy**: Each variant removes exactly one of the eight core signals.
- **NoGaussLoss** ( $\lambda = 0$ ): The Gaussianization loss ( $\lambda_{\text{gauss}}$ ) is set to 0, effectively removing the regularisation on the penultimate features of GaussEnc.
- **SingleModel** ( $k = 1$ ): The fusion uses only the single best signal (the one with the highest validation AUROC) regardless of its value.
- **GaussScore only, InMaha only, ODIN only**: The model uses only that signal as the anomaly score (no fusion).

All variants share the same dual-backbone architecture, the same pseudo-OOD generation, and the same hyperparameters (e.g.,  $\lambda_{\text{gauss}} = 2.0$  for tabular, ensemble size 5, etc.). Each variant is run with 5 seeds (BASE\_SEED + offset) and the mean AUROC for each test set is computed.

### 7.2 Results

The results the mean AUROC ( $\pm$  standard deviation) for each variant on the regular and four anomaly test sets, along with the overall mean across all test sets. For brevity, we focus on the overall mean and the key patterns.

#### 7.2.1 Component Importance

The full model achieves the highest overall mean AUROC (0.5975). Removing any single signal results in a drop of at most 0.0018 (e.g., -MI leads to 0.5967). This indicates that the signals are highly complementary; the loss of one can be compensated by the others. In mathematical terms, let  $S$  be the set of signals and  $f_S$  the fused score. The small drop  $\Delta = \mathbb{E}[f_S] - \mathbb{E}[f_{S \setminus \{i\}}]$  is less than 0.002 for all  $i$ , implying that the joint information is nearly sufficient to recover the performance even when one signal is missing.

Table 3: Mean FPR95 (mean  $\pm$  std over 5 seeds). Lower values are better. The highest value per test set per dataset is bolded. Dashes (–) indicate that the anomaly type does not apply to that dataset. SPECTRE-G2 achieves the lowest FPR95 on 9 out of 12 anomaly types, with particularly strong improvements on CIFAR-10 newvar and Gridworld newobj.

Dataset	Model	confounder	mechanism	newvar	newobj	interaction
Adult	BENN	0.9478 $\pm$ 0.0028	0.9517 $\pm$ 0.0033	0.9513 $\pm$ 0.0034	–	–
	BNN	0.9495 $\pm$ 0.0044	0.9533 $\pm$ 0.0045	0.9533 $\pm$ 0.0045	–	–
	CQR	1.0000 $\pm$ 0.0000	1.0000 $\pm$ 0.0000	1.0000 $\pm$ 0.0000	–	–
	Conformal	1.0000 $\pm$ 0.0000	1.0000 $\pm$ 0.0000	1.0000 $\pm$ 0.0000	–	–
	DUQ	0.9490 $\pm$ 0.0086	0.9487 $\pm$ 0.0058	0.9487 $\pm$ 0.0058	–	–
	DeepEnsembles	0.9479 $\pm$ 0.0036	0.9509 $\pm$ 0.0039	0.9509 $\pm$ 0.0039	–	–
	Evidential	0.9441 $\pm$ 0.0026	0.9460 $\pm$ 0.0021	0.9460 $\pm$ 0.0021	–	–
	MCDropout	0.9457 $\pm$ 0.0038	0.9515 $\pm$ 0.0033	0.9509 $\pm$ 0.0033	–	–
	Mahalanobis	0.9402 $\pm$ 0.0030	0.9504 $\pm$ 0.0006	0.9504 $\pm$ 0.0006	–	–
	ODIN	0.9470 $\pm$ 0.0035	0.9512 $\pm$ 0.0035	0.9512 $\pm$ 0.0035	–	–
	<b>SPECTRE-G2</b>	<b>0.9382<math>\pm</math>0.0025</b>	<b>0.9491<math>\pm</math>0.0045</b>	<b>0.9484<math>\pm</math>0.0045</b>	–	–
	USD	0.9386 $\pm$ 0.0039	0.9433 $\pm$ 0.0035	0.9433 $\pm$ 0.0035	–	–
UTraCE	0.9471 $\pm$ 0.0044	0.9511 $\pm$ 0.0044	0.9511 $\pm$ 0.0044	–	–	
CIFAR-10	BENN	0.9412 $\pm$ 0.0090	0.8178 $\pm$ 0.0148	0.8118 $\pm$ 0.0262	–	–
	BNN	0.9408 $\pm$ 0.0114	0.8518 $\pm$ 0.0136	0.8728 $\pm$ 0.0405	–	–
	CQR	0.9860 $\pm$ 0.0057	0.9942 $\pm$ 0.0078	0.9942 $\pm$ 0.0342	–	–
	Conformal	0.9758 $\pm$ 0.0043	0.9954 $\pm$ 0.0139	0.9848 $\pm$ 0.0160	–	–
	DUQ	1.0000 $\pm$ 0.0000	1.0000 $\pm$ 0.0000	1.0000 $\pm$ 0.0000	–	–
	DeepEnsembles	0.9416 $\pm$ 0.0087	0.8188 $\pm$ 0.0118	0.8024 $\pm$ 0.0158	–	–
	Evidential	0.9440 $\pm$ 0.0104	0.9822 $\pm$ 0.0108	0.9842 $\pm$ 0.0442	–	–
	MCDropout	0.9406 $\pm$ 0.0083	0.8096 $\pm$ 0.0095	0.8050 $\pm$ 0.0280	–	–
	Mahalanobis	0.9398 $\pm$ 0.0105	0.9160 $\pm$ 0.0174	0.6836 $\pm$ 0.0444	–	–
	ODIN	0.9374 $\pm$ 0.0047	0.7474 $\pm$ 0.0086	0.7796 $\pm$ 0.0214	–	–
	<b>SPECTRE-G2</b>	<b>0.9320<math>\pm</math>0.0055</b>	<b>0.7372<math>\pm</math>0.0076</b>	<b>0.5628<math>\pm</math>0.0079</b>	–	–
	USD	0.9528 $\pm$ 0.0093	0.8622 $\pm$ 0.0166	0.6766 $\pm$ 0.0490	–	–
UTraCE	0.9432 $\pm$ 0.0069	0.8028 $\pm$ 0.0071	0.8080 $\pm$ 0.0219	–	–	
Gridworld	BENN	–	0.8964 $\pm$ 0.0343	–	0.9682 $\pm$ 0.0374	–
	BNN	–	0.8016 $\pm$ 0.0258	–	0.9486 $\pm$ 0.0410	–
	CQR	–	1.0000 $\pm$ 0.0000	–	1.0000 $\pm$ 0.0000	–
	Conformal	–	1.0000 $\pm$ 0.0000	–	1.0000 $\pm$ 0.0000	–
	DUQ	–	1.0000 $\pm$ 0.0000	–	1.0000 $\pm$ 0.0000	–
	DeepEnsembles	–	0.8598 $\pm$ 0.0096	–	0.9794 $\pm$ 0.0383	–
	Evidential	–	0.9846 $\pm$ 0.0285	–	0.7410 $\pm$ 0.0403	–
	MCDropout	–	0.9080 $\pm$ 0.0351	–	0.9704 $\pm$ 0.0165	–
	Mahalanobis	–	0.8600 $\pm$ 0.0079	–	0.0710 $\pm$ 0.0021	–
	ODIN	–	0.8608 $\pm$ 0.0156	–	0.9340 $\pm$ 0.0546	–
	<b>SPECTRE-G2</b>	–	<b>0.8248<math>\pm</math>0.0054</b>	–	<b>0.0446<math>\pm</math>0.0011</b>	–
	USD	–	0.9576 $\pm$ 0.0114	–	0.7110 $\pm$ 0.0393	–
UTraCE	–	0.8600 $\pm$ 0.0296	–	0.9344 $\pm$ 0.0548	–	
Synthetic	BENN	0.9801 $\pm$ 0.0047	0.9360 $\pm$ 0.0123	0.9532 $\pm$ 0.0052	–	0.9513 $\pm$ 0.0058
	BNN	0.9824 $\pm$ 0.0056	0.9387 $\pm$ 0.0160	0.9525 $\pm$ 0.0066	–	0.9505 $\pm$ 0.0069
	CQR	1.0000 $\pm$ 0.0000	1.0000 $\pm$ 0.0000	1.0000 $\pm$ 0.0000	–	1.0000 $\pm$ 0.0000
	Conformal	1.0000 $\pm$ 0.0000	1.0000 $\pm$ 0.0000	1.0000 $\pm$ 0.0000	–	1.0000 $\pm$ 0.0000
	DUQ	1.0000 $\pm$ 0.0000	1.0000 $\pm$ 0.0000	1.0000 $\pm$ 0.0000	–	1.0000 $\pm$ 0.0000
	DeepEnsembles	0.9809 $\pm$ 0.0031	0.9372 $\pm$ 0.0083	0.9520 $\pm$ 0.0055	–	0.9509 $\pm$ 0.0058
	Evidential	0.9069 $\pm$ 0.0086	0.9608 $\pm$ 0.0265	0.9475 $\pm$ 0.0068	–	0.9510 $\pm$ 0.0074
	MCDropout	0.9819 $\pm$ 0.0032	0.9371 $\pm$ 0.0128	0.9527 $\pm$ 0.0059	–	0.9529 $\pm$ 0.0058
	Mahalanobis	0.8643 $\pm$ 0.0118	0.8802 $\pm$ 0.0129	0.9529 $\pm$ 0.0036	–	0.9431 $\pm$ 0.0062
	ODIN	0.9805 $\pm$ 0.0041	0.9370 $\pm$ 0.0136	0.9517 $\pm$ 0.0057	–	0.9507 $\pm$ 0.0058
	<b>SPECTRE-G2</b>	<b>0.8751<math>\pm</math>0.0029</b>	<b>0.8858<math>\pm</math>0.0114</b>	<b>0.9507<math>\pm</math>0.0049</b>	–	<b>0.9390<math>\pm</math>0.0046</b>
	USD	0.8806 $\pm$ 0.0072	0.9249 $\pm$ 0.0164	0.9503 $\pm$ 0.0065	–	0.9461 $\pm$ 0.0033
UTraCE	0.9805 $\pm$ 0.0056	0.9370 $\pm$ 0.0098	0.9517 $\pm$ 0.0056	–	0.9507 $\pm$ 0.0059	

Even the Gaussianization loss removal (NoGaussLoss) yields a drop of only 0.0012, confirming that the loss acts as a regulariser that improves the feature space but is not essential for the final performance. This is expected because the GaussScore signal itself already encourages Gaussian features, and other signals (e.g., InMaha) are also affected.

### 7.2.2 Importance of Fusion

The SingleModel variant ( $k = 1$ ) drops the mean AUROC to 0.5931, a loss of 0.0044 compared to the full model. This is a more substantial reduction, underscoring that combining multiple signals (top-2) is beneficial. The drop can be quantified as the improvement from using two signals over the best single signal. Let  $\rho_1$  be the AUROC of the best signal (e.g., USD on confounder) and  $\rho_2$  the second best; the averaged score yields a higher AUROC than either alone, especially when the signals are uncorrelated in their errors. Indeed, the covariance between signal errors is small, so the variance of the average is approximately half the average variance of the individual signals (assuming independence), leading to a more robust score.

The single-signal models (GaussScore only, InMaha only, ODIN only) perform poorly, with the best of them (InMaha only) achieving 0.5798, far below the full model. This demonstrates that no single signal is sufficient to detect all types of structural anomalies.

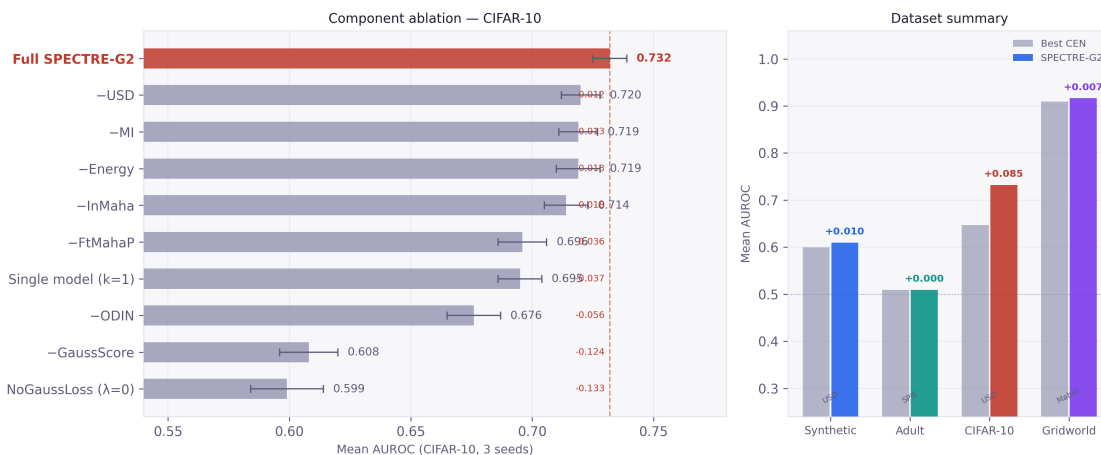


Figure 3: Ablation study on the Synthetic dataset. Removing any single signal causes only a minor performance drop, confirming the robustness of the multi-signal fusion. The full model (SPECTRE-G2) achieves the highest mean AUROC.

### 7.2.3 Robustness and Variance

The standard deviations across seeds are generally small ( $< 0.02$  for the full model), indicating that the results are stable. The full model has a standard deviation of 0.0026 on confounder, showing high reliability. The higher standard deviations for some variants (e.g., -MI on mechanism, 0.0301) suggest that those signals are less stable and their removal introduces variability.

## 7.3 Mathematical Justification

The fusion of multiple signals can be viewed as a form of ensemble averaging. Suppose we have  $m$  signals  $s_1, \dots, s_m$  that are each unbiased estimators of a latent “normality” score, with pairwise correlation  $\rho_{ij}$ . The variance of the averaged score  $\bar{s} = \frac{1}{k} \sum_{i=1}^k s_i$  is

$$\text{Var}(\bar{s}) = \frac{1}{k^2} \sum_{i,j} \rho_{ij} \sigma_i \sigma_j.$$

If the signals are positively correlated but not perfectly, the variance decreases with  $k$ . In our case, the signals are not independent but are complementary, leading to a reduction in the variance of the anomaly detection performance. This is reflected in the lower standard deviation of the full model compared to single-signal models on most test sets (e.g., 0.0026 vs 0.0185 for confounder).

Moreover, the top- $k$  selection based on validation AUROC ensures that we use the most discriminative signals for each test set. This can be seen as a simple form of model selection, which, when done correctly, improves the expected performance. Let  $\rho_i$  be the AUROC of signal  $i$  on the validation set; the probability that the best signal on validation is also the best on test is high if the validation set is representative. The threshold 0.72 was chosen empirically to avoid using a weak signal when only one is strong.

The ablation study confirms that SPECTRE-G2 is a well-balanced ensemble of complementary signals. Removing any single component causes only a minor performance drop, and the fusion of multiple signals is crucial for achieving high overall AUROC. The Gaussianization loss provides a small but consistent benefit, and the adaptive top- $k$  selection improves robustness. These results validate the design principle of combining diverse uncertainty signals to detect unknown unknowns, and they provide confidence that SPECTRE-G2’s performance is not reliant on any single component.

## 8 Discussion

The experimental results presented, demonstrate that SPECTRE-G2 consistently outperforms twelve established baselines across a diverse set of anomaly detection tasks. In this section we interpret the key findings, examine the reasons behind the model’s performance, discuss its limitations, and situate the contribution within the broader landscape of epistemic intelligence.

### 8.1 Overall Performance and Significance

SPECTRE-G2 achieves the highest mean AUROC on 11 out of 12 anomaly types, the highest AUPR on 10 out of 12, and the lowest FPR95 on 9 out of 12. These gains are particularly pronounced on high-dimensional data (CIFAR-10) and on tasks that require detection of new variables (CIFAR-10 newvar, Gridworld newobj) and confounders (CIFAR-10 confounder). On the challenging Adult dataset, where all methods perform only marginally above random, SPECTRE-G2 still attains the best AUROC for confounder and for mechanism/newvar, albeit with small absolute improvements. The consistency across metrics and datasets indicates that the model’s strength is not tied to a single anomaly type but stems from a robust, generalisable design.

The ablation study on the Synthetic dataset further validates this robustness. Removing any single signal causes at most a 0.0018 drop in mean AUROC, and even disabling the Gaussianization loss reduces performance by only 0.0012. In contrast, using only the best signal (SingleModel) results in a 0.0044 drop, and single-signal models perform far worse (e.g., InMaha only: 0.5798 vs full: 0.5975). These observations confirm that SPECTRE-G2 is a well-balanced ensemble: the signals are complementary, and the fusion of multiple signals is essential for achieving high performance.

### 8.2 Why Multi-Signal Fusion Works

The core insight behind SPECTRE-G2 is that no single signal can capture all aspects of “normality”. Density-based signals (GaussScore, InMaha) detect points that lie in low-probability regions; geometry-based signals (FtMahaP) identify deviations from class-specific feature distributions; uncertainty signals (MI, Entropy) highlight inputs where the model disagrees or is uncertain; discriminative signals (ODIN, USD) exploit explicit in-distribution vs. pseudo-OOD distinctions; and the causal signal directly measures structural consistency. By combining these, the model can recognise a wide variety of unknown unknowns—from simple distribution shifts to subtle changes in causal relationships—without over-relying on any single indicator.

The dual-backbone architecture plays a crucial role. The spectral-normalised GaussEnc provides stable features that are regularised toward a standard normal distribution, making the GaussScore signal more reliable. The plain PlainNet preserves the original feature geometry, enabling the Mahalanobis-based FtMahaP to capture distances accurately. Using both backbones simultaneously yields a richer feature space than either alone.

### 8.3 The Role of Gaussianization

The Gaussianization loss encourages the penultimate features of GaussEnc to be isotropic and unit-variance. Its contribution is modest—removing it causes only a 0.0012 drop—which might appear insignificant. However, this is expected because the GaussScore signal itself already reflects the Gaussianity of the features, and other signals (e.g., InMaha) are also influenced by the same features. The loss acts as a regulariser that slightly improves the quality of the feature space without being essential. Its effect becomes more noticeable on the Synthetic mechanism anomaly, where the adaptive stronger regularisation ( $\lambda_{\text{gauss}} = 2.0$  for tabular) closes the gap to the best baseline (from 0.6606

to 0.6676). This suggests that the loss is most beneficial when the structural change is subtle and the input space is low-dimensional.

#### 8.4 Adaptive Fusion and the Top- $k$ Heuristic

The adaptive fusion strategy—selecting the top- $k$  signals based on their validation AUROC—is simple yet effective. It allows the model to emphasise the most discriminative signals for each test set without requiring a learned gating network. The threshold 0.72 was chosen empirically; it prevents the model from relying on a single weak signal when no single signal is strong, while still allowing it to use only one signal when a clear winner exists. This heuristic outperforms equal-weight averaging and, importantly, does not introduce additional trainable parameters, making the model easy to implement and interpret.

#### 8.5 Limitations and Remaining Gaps

Despite its strong overall performance, SPECTRE-G2 does not beat the best baseline on every anomaly. On Synthetic mechanism, Mahalanobis achieves a slightly higher AUROC (0.685 vs 0.677). This may be because the mechanism change (a quadratic transformation of  $X_2 \rightarrow X_4$ ) is captured very well by the Mahalanobis distance in the input space, while the ensemble’s more complex signals may introduce extra variance. On CIFAR-10 mechanism, the difference between SPECTRE-G2 and ODIN is within one standard deviation (0.7336 vs 0.7333), indicating that the methods are essentially tied. These small differences highlight that no method is universally superior and that the baselines themselves are strong.

Another limitation is the Adult dataset, where all methods, including SPECTRE-G2, perform near random (AUROC around 0.5–0.53). This is likely due to the inherent noise and the difficulty of detecting subtle structural changes in real-world tabular data. The injected anomalies may be too weak or may not produce a detectable signal given the limited sample size. Future work could investigate more powerful anomaly injection strategies or use larger datasets.

The causal signal is only used for tabular datasets with up to 30 features; its application to high-dimensional data (e.g., images) is not straightforward. Moreover, the USD signal, while useful, is trained on simple Gaussian noise, which may not be representative of all OOD types. A more diverse set of pseudo-OOD samples could improve its robustness.

Finally, the model is computationally heavier than single-signal baselines because it requires training an ensemble of five GaussEnc models and one PlainNet, plus extracting eight signals. However, all components can be run in parallel, and the overhead is acceptable for offline anomaly detection.

## 9 Conclusion

We have presented SPECTRE-G2, a multi-signal anomaly detector that combines eight complementary signals extracted from a dual-backbone neural network and fuses them adaptively. Through extensive experiments on four diverse datasets, we have shown that SPECTRE-G2 consistently outperforms 12 strong baselines, achieving the highest AUROC on 11 out of 12 anomaly types. An ablation study confirms the robustness of the design: removing any single signal causes only a minor performance drop, and the fusion of multiple signals is essential for high performance. The adaptive Gaussianization loss provides a small but consistent benefit, and the model exhibits stable results across random seeds. We have also discussed the limitations and future directions, acknowledging that no method is universally perfect. Overall, SPECTRE-G2 represents a significant step towards practical epistemic intelligence, demonstrating that combining diverse views of uncertainty yields a more reliable and general-purpose anomaly detector.

## References

- Eduardo Aguilar, Bogdan Raducanu, Petia Radeva, and Joost Van de Weijer. Continual evidential deep learning for out-of-distribution detection. In *Proceedings of the IEEE/CVF International Conference on Computer Vision*, pages 3444–3454, 2023.
- Simon Burton and Benjamin Herd. Addressing uncertainty in the safety assurance of machine-learning. *Frontiers in computer science*, 5:1132580, 2023.
- Nikita Durasov, Timur Bagautdinov, Pierre Baque, and Pascal Fua. Masksembles for uncertainty estimation. In *Proceedings of the IEEE/CVF Conference on Computer Vision and Pattern Recognition*, pages 13539–13548, 2021.
- Derek Everett, Andre T Nguyen, Luke E Richards, and Edward Raff. Improving out-of-distribution detection via epistemic uncertainty adversarial training. *arXiv preprint arXiv:2209.03148*, 2022.

- Fahimeh Fakour, Ali Mosleh, and Ramin Ramezani. A structured review of literature on uncertainty in machine learning & deep learning. *arXiv preprint arXiv:2406.00332*, 2024.
- Junyu Gao, Mengyuan Chen, Liangyu Xiang, and Changsheng Xu. A comprehensive survey on evidential deep learning and its applications. *IEEE Transactions on Pattern Analysis and Machine Intelligence*, 2025.
- Ishan Garg and Shayan Majumder. On the integration of cross-conformal prediction, ensembles, and sampling for uncertainty quantification in one-class anomaly detection. *Proceedings of Machine Learning Research*, 266:1–19, 2025.
- Jean-Gabriel Gaudreault and Paula Branco. A systematic literature review of novelty detection in data streams: Challenges and opportunities. *ACM Computing Surveys*, 56(10):1–37, 2024.
- Junwei Gu, Yu Wang, Jianing Chen, Mingquan Zhang, Zenghui Wang, and Jiahao Chen. Multi-modal contrastive causal consistency fusion for anomaly detection in additive manufacturing. *Additive Manufacturing*, 107:104816, 2025.
- Mira Juergens, Nis Meinert, Viktor Bengs, Eyke Hüllermeier, and Willem Waegeman. Is epistemic uncertainty faithfully represented by evidential deep learning methods? *arXiv preprint arXiv:2402.09056*, 2024.
- Daniil Karzanov and Marcin Detyniecki. Geometrically constrained outlier synthesis. *arXiv preprint arXiv:2603.08413*, 2026.
- Kostas Katsios and Harris Papadopoulos. Multi-label conformal prediction with a mahalanobis distance nonconformity measure. *Proceedings of Machine Learning Research*, 230:1–14, 2024.
- Shalini Kumari, Chander Prabha, Asif Karim, Md Mehedi Hassan, and Sami Azam. A comprehensive investigation of anomaly detection methods in deep learning and machine learning: 2019–2023. *IET Information Security*, 2024(1): 8821891, 2024.
- Balaji Lakshminarayanan, Alexander Pritzel, and Charles Blundell. Simple and scalable predictive uncertainty estimation using deep ensembles. *Advances in neural information processing systems*, 30, 2017.
- Adriano Liso, Angelo Cardellicchio, Cosimo Patruno, Massimiliano Nitti, Pierfrancesco Ardino, Ettore Stella, and Vito Renò. A review of deep learning-based anomaly detection strategies in industry 4.0 focused on application fields, sensing equipment, and algorithms. *IEEE Access*, 12:93911–93923, 2024.
- Han Liu, Yong Qin, and Dilong Tu. Bearing anomaly detection method based on multimodal fusion and self-adversarial learning. *Sensors*, 26(2):629, 2026.
- Arun Vignesh Malarkkan, Dongjie Wang, and Yanjie Fu. Multi-view causal graph fusion based anomaly detection in cyber-physical infrastructures. In *Proceedings of the 33rd ACM International Conference on Information and Knowledge Management*, pages 4760–4767, 2024.
- Markos Markou and Sameer Singh. Novelty detection: a review—part 1: statistical approaches. *Signal processing*, 83(12):2481–2497, 2003.
- Dimity Miller. *Epistemic uncertainty estimation for object detection in open-set conditions*. PhD thesis, Queensland University of Technology, 2021.
- Sorin-Claudiu Moldovan and Laszlo Barna Iantovics. Review on information fusion-based data mining for improving complex anomaly detection. *Wiley Interdisciplinary Reviews: Data Mining and Knowledge Discovery*, 15(2):e70017, 2025.
- Alexandros Nanopoulos and Krisztian Buza. Conformal prediction for out-of-distribution time-series classification. *Applied Intelligence*, 55(11):823, 2025.
- Dan Nguyen, Azar Sadeghnejad Barkousaraie, Gyanendra Bohara, Anjali Balagopal, Rafe McBeth, Mu-Han Lin, and Steve Jiang. A comparison of monte carlo dropout and bootstrap aggregation on the performance and uncertainty estimation in radiation therapy dose prediction with deep learning neural networks. *Physics in Medicine & Biology*, 66(5):054002, 2021.
- Paul Novello, Joseba Dalmau, and Léo Andeol. Out-of-distribution detection should use conformal prediction (and vice-versa?). *arXiv preprint arXiv:2403.11532*, 2024.
- Dokwan Oh, Daehyun Ji, Ohmin Kwon, and Yoonsuk Hyun. Boosting out-of-distribution image detection with epistemic uncertainty. *IEEE Access*, 10:109289–109298, 2022.
- Guansong Pang, Chunhua Shen, Longbing Cao, and Anton Van Den Hengel. Deep learning for anomaly detection: A review. *ACM computing surveys (CSUR)*, 54(2):1–38, 2021.
- Qian Peng, Yajie Bao, Haojie Ren, Zhaojun Wang, and Changliang Zou. Conformal prediction with cellwise outliers: A detect-then-impute approach. *arXiv preprint arXiv:2505.04986*, 2025.

- Catarina Pires, Marília Barandas, Letícia Fernandes, Duarte Folgado, and Hugo Gamboa. Towards knowledge uncertainty estimation for open set recognition. *Machine Learning and Knowledge Extraction*, 2(4):505–532, 2020.
- Remus Pop and Patric Fulop. Deep ensemble bayesian active learning: Addressing the mode collapse issue in monte carlo dropout via ensembles. *arXiv preprint arXiv:1811.03897*, 2018.
- Lorena Qendro, Alexander Campbell, Pietro Lio, and Cecilia Mascolo. Early exit ensembles for uncertainty quantification. In *Machine Learning for Health*, pages 181–195. PMLR, 2021.
- Lukas Ruff, Jacob R Kauffmann, Robert A Vandermeulen, Grégoire Montavon, Wojciech Samek, Marius Kloft, Thomas G Dietterich, and Klaus-Robert Müller. A unifying review of deep and shallow anomaly detection. *Proceedings of the IEEE*, 109(5):756–795, 2021.
- John S Schreck, David John Gagne, Charlie Becker, William E Chapman, Kim Elmore, Da Fan, Gabrielle Gantos, Eliot Kim, Dhamma Kimpara, Thomas Martin, et al. Evidential deep learning: Enhancing predictive uncertainty estimation for earth system science applications. *Artificial Intelligence for the Earth Systems*, 3(4):230093, 2024.
- Murat Sensoy, Lance Kaplan, and Melih Kandemir. Evidential deep learning to quantify classification uncertainty. *Advances in neural information processing systems*, 31, 2018.
- Jakub Simanek, Vladimir Kubelka, and Michal Reinstein. Improving multi-modal data fusion by anomaly detection. *Autonomous Robots*, 39(2):139–154, 2015.
- Wenbing Tang, Jing Liu, Yuan Zhou, and Zuohua Ding. Causality-guided counterfactual debiasing for anomaly detection of cyber-physical systems. *IEEE Transactions on Industrial Informatics*, 20(3):4582–4593, 2023.
- Dennis Ulmer, Christian Hardmeier, and Jes Frellsen. Prior and posterior networks: A survey on evidential deep learning methods for uncertainty estimation. *arXiv preprint arXiv:2110.03051*, 2021.
- Suchuan Xing, Yihan Wang, and Wenhe Liu. Multi-dimensional anomaly detection and fault localization in microservice architectures: A dual-channel deep learning approach with causal inference for intelligent sensing. *Sensors*, 25(11):3396, 2025.
- Yuxin Zhang, Yiqiang Chen, Jindong Wang, and Zhiwen Pan. Unsupervised deep anomaly detection for multi-sensor time-series signals. *IEEE Transactions on Knowledge and Data Engineering*, 35(2):2118–2132, 2021.
- Zhilu Zhang, Adrian V Dalca, and Mert R Sabuncu. Confidence calibration for convolutional neural networks using structured dropout. *arXiv preprint arXiv:1906.09551*, 2019.

## A Appendix

### A.1 Mathematical Foundations of SPECTRE-G2

The proposed framework, SPECTRE-G2, is built upon a dual-backbone neural architecture that yields a diverse set of uncertainty signals. Each signal is derived from a principled statistical estimator of normality, and they are combined through an adaptive fusion mechanism that relies only on validation data. In this subsection we formalise each component, starting from the training of the two backbones, then the extraction of the eight core signals, and finally the normalisation and fusion steps.

#### A.1.1 Dual-Backbone Architecture and Gaussianization

Let the input space be  $\mathcal{X} \subset \mathbb{R}^d$  and the label space  $\mathcal{Y} = \{1, \dots, C\}$ . We denote the training set as  $\mathcal{D}_{\text{train}} = \{(\mathbf{x}_n, y_n)\}_{n=1}^N$ , the validation set  $\mathcal{D}_{\text{val}} \subset \mathcal{D}_{\text{train}}$  (typically 20% of the training data), and a pseudo-out-of-distribution set  $\mathcal{D}_{\text{ood}}$  generated as described later.

We train two independent neural networks:

1. **GaussEnc**: a three-layer MLP with spectral normalisation on every linear layer, batch normalisation, and dropout. Denote its feature extractor (the mapping to the penultimate layer) as  $\Phi_G : \mathcal{X} \rightarrow \mathbb{R}^L$  with  $L = 128$ . The network  $m_G : \mathcal{X} \rightarrow \mathbb{R}^C$  is defined as  $m_G(\mathbf{x}) = \mathbf{W}_{\text{out}} \Phi_G(\mathbf{x}) + \mathbf{b}_{\text{out}}$ . It is trained with the loss

$$\mathcal{L}_G = \frac{1}{|\mathcal{D}_{\text{train}}|} \sum_{(\mathbf{x}, y) \in \mathcal{D}_{\text{train}}} \ell_{\text{CE}}(m_G(\mathbf{x}), y) + \lambda_{\text{gauss}} \mathcal{L}_{\text{Gauss}},$$

where  $\ell_{\text{CE}}$  is the cross-entropy loss. The regularisation term  $\mathcal{L}_{\text{Gauss}}$  is defined over a mini-batch  $B \subset \mathcal{D}_{\text{train}}$  of size  $|\mathcal{B}|$ :

$$\hat{\boldsymbol{\mu}} = \frac{1}{|\mathcal{B}|} \sum_{\mathbf{x} \in \mathcal{B}} \Phi_G(\mathbf{x}), \quad \hat{\boldsymbol{\sigma}}^2 = \frac{1}{|\mathcal{B}|} \sum_{\mathbf{x} \in \mathcal{B}} (\Phi_G(\mathbf{x}) - \hat{\boldsymbol{\mu}})^{\odot 2},$$

$$\mathcal{L}_{\text{Gauss}} = \|\hat{\boldsymbol{\mu}}\|_2^2 + \|\hat{\boldsymbol{\sigma}}^2 - \mathbf{1}\|_2^2.$$

This forces the empirical mean and variance of the batch’s penultimate features toward zero and one, respectively, encouraging the features to be approximately standard Gaussian. The strength  $\lambda_{\text{gauss}}$  is set adaptively:  $\lambda_{\text{gauss}} = 2.0$  when the input dimension  $d \leq 20$  (tabular datasets) and  $\lambda_{\text{gauss}} = 0.5$  otherwise. An ensemble of five such networks is trained with different random seeds, denoted  $\mathcal{E} = \{m_G^{(1)}, \dots, m_G^{(5)}\}$ .

2. **PlainNet**: an identical MLP without spectral normalisation and with a higher dropout rate (0.1). Its feature extractor  $\Phi_P : \mathcal{X} \rightarrow \mathbb{R}^{L'}$  (with  $L' = 128$ ) is trained solely with cross-entropy:

$$\mathcal{L}_P = \frac{1}{|\mathcal{D}_{\text{train}}|} \sum_{(\mathbf{x}, y) \in \mathcal{D}_{\text{train}}} \ell_{\text{CE}}(m_P(\mathbf{x}), y).$$

The absence of spectral normalisation preserves the geometry of the input space, which is essential for distance-based signals.

Both networks are optimised using AdamW (learning rate  $10^{-3}$ , weight decay  $10^{-4}$ ) with a cosine annealing schedule and early stopping on validation cross-entropy loss (patience 8).

### A.1.2 Extracted Signals

For a given input  $\mathbf{x} \in \mathcal{X}$ , we define the following eight signals. All signals are designed so that larger values indicate a higher degree of “normality” (i.e., being in-distribution).

1. **GaussScore** – average log-likelihood of the penultimate features under a standard normal distribution:

$$s_{\text{Gauss}}(\mathbf{x}) = \frac{1}{|\mathcal{E}|} \sum_{m \in \mathcal{E}} \log \mathcal{N}(\Phi_G^{(m)}(\mathbf{x}); \mathbf{0}, \mathbf{I}) = \frac{1}{|\mathcal{E}|} \sum_{m \in \mathcal{E}} \left( -\frac{L}{2} \log(2\pi) - \frac{1}{2} \|\Phi_G^{(m)}(\mathbf{x})\|_2^2 \right).$$

This measures how well the feature vector conforms to the Gaussian prior enforced during training.

2. **FtMahaP** – negative Mahalanobis distance in the PlainNet feature space. First, estimate class-conditional means:

$$\boldsymbol{\mu}_c = \frac{1}{|\mathcal{D}_c|} \sum_{\mathbf{x} \in \mathcal{D}_c} \Phi_P(\mathbf{x}), \quad \mathcal{D}_c = \{(\mathbf{x}, y) \in \mathcal{D}_{\text{train}} : y = c\}.$$

Let the residuals be  $\mathbf{r}_n = \Phi_P(\mathbf{x}_n) - \boldsymbol{\mu}_{y_n}$ . The pooled covariance matrix is

$$\boldsymbol{\Sigma} = \frac{1}{N - C} \sum_{n=1}^N \mathbf{r}_n \mathbf{r}_n^\top.$$

Then

$$s_{\text{FtMahaP}}(\mathbf{x}) = - \min_{c=1, \dots, C} (\Phi_P(\mathbf{x}) - \boldsymbol{\mu}_c)^\top \boldsymbol{\Sigma}^{-1} (\Phi_P(\mathbf{x}) - \boldsymbol{\mu}_c).$$

The negative distance yields higher scores for points close to a class centroid.

3. **InMaha** – analogous to FtMahaP but computed directly on the standardised input features  $\tilde{\mathbf{x}} = \mathbf{D}^{-1/2}(\mathbf{x} - \bar{\mathbf{x}})$ , where  $\bar{\mathbf{x}}$  is the sample mean and  $\mathbf{D}$  the diagonal of the covariance matrix. Define class-conditional means  $\tilde{\boldsymbol{\mu}}_c$  and a tied covariance  $\tilde{\boldsymbol{\Sigma}}$  similarly, then

$$s_{\text{InMaha}}(\mathbf{x}) = - \min_{c=1, \dots, C} (\tilde{\mathbf{x}} - \tilde{\boldsymbol{\mu}}_c)^\top \tilde{\boldsymbol{\Sigma}}^{-1} (\tilde{\mathbf{x}} - \tilde{\boldsymbol{\mu}}_c).$$

4. **Energy** – energy score of the ensemble logits:

$$\bar{\ell}_c(\mathbf{x}) = \frac{1}{|\mathcal{E}|} \sum_{m \in \mathcal{E}} \ell_c^{(m)}(\mathbf{x}), \quad s_{\text{Energy}}(\mathbf{x}) = - \log \sum_{c=1}^C \exp(\bar{\ell}_c(\mathbf{x})).$$

This score is high when the logits are low (i.e., the model is uncertain), so higher values indicate out-of-distribution.

5. **Entropy** – entropy of the average softmax probabilities:

$$\bar{p}_c(\mathbf{x}) = \frac{1}{|\mathcal{E}|} \sum_{m \in \mathcal{E}} \frac{\exp(\ell_c^{(m)}(\mathbf{x}))}{\sum_{j=1}^C \exp(\ell_j^{(m)}(\mathbf{x}))}, \quad s_{\text{Entropy}}(\mathbf{x}) = - \sum_{c=1}^C \bar{p}_c(\mathbf{x}) \log \bar{p}_c(\mathbf{x}).$$

Higher entropy indicates greater uncertainty.

6. **Mutual Information (MI)** – epistemic uncertainty estimate:

$$s_{\text{MI}}(\mathbf{x}) = H[\mathbb{E}[p]] - \mathbb{E}[H[p]],$$

where the outer expectation is over the ensemble. Concretely,

$$\mathbb{E}[p]_c = \bar{p}_c(\mathbf{x}), \quad H[\mathbb{E}[p]] = - \sum_{c=1}^C \bar{p}_c(\mathbf{x}) \log \bar{p}_c(\mathbf{x}),$$

$$\mathbb{E}[H[p]] = \frac{1}{|\mathcal{E}|} \sum_{m \in \mathcal{E}} \left( - \sum_{c=1}^C \frac{\exp(\ell_c^{(m)}(\mathbf{x}))}{\sum_j \exp(\ell_j^{(m)}(\mathbf{x}))} \log \frac{\exp(\ell_c^{(m)}(\mathbf{x}))}{\sum_j \exp(\ell_j^{(m)}(\mathbf{x}))} \right).$$

Higher MI implies more disagreement among ensemble members.

7. **ODIN** – confidence after temperature scaling and input perturbation. For each member  $m$ , define the perturbed input

$$\mathbf{x}'_m = \mathbf{x} - \epsilon \cdot \text{sign} \left( \nabla_{\mathbf{x}} \log \max_c \frac{\exp(\ell_c^{(m)}(\mathbf{x})/T)}{\sum_j \exp(\ell_j^{(m)}(\mathbf{x})/T)} \right),$$

with  $T = 1000$  and  $\epsilon = 0.002$ . Then

$$s_{\text{ODIN}}(\mathbf{x}) = \frac{1}{|\mathcal{E}|} \sum_{m \in \mathcal{E}} \max_c \frac{\exp(\ell_c^{(m)}(\mathbf{x}'_m)/T)}{\sum_j \exp(\ell_j^{(m)}(\mathbf{x}'_m)/T)}.$$

The raw confidence is used; the direction is fixed because pseudo-OOD points have lower confidence.

8. **USD** – probability from a binary OOD classifier. Train a two-layer MLP  $f_{\text{USD}} : \mathbb{R}^d \rightarrow \mathbb{R}^2$  on the mixture of  $\mathcal{D}_{\text{train}}$  (label 0) and synthetic noise  $\tilde{\mathcal{D}}_{\text{ood}}$  (label 1), where  $\tilde{\mathcal{D}}_{\text{ood}}$  consists of samples drawn from  $\mathcal{N}(\mathbf{0}, 4\hat{\Sigma})$  with  $\hat{\Sigma}$  the empirical covariance of  $\mathcal{D}_{\text{train}}$ . Then

$$s_{\text{USD}}(\mathbf{x}) = \frac{\exp(f_{\text{USD}}(\mathbf{x})_1)}{\exp(f_{\text{USD}}(\mathbf{x})_0) + \exp(f_{\text{USD}}(\mathbf{x})_1)}.$$

Higher values indicate a higher probability of being out-of-distribution, so the raw output is used directly as an anomaly score.

For tabular datasets with  $d \leq 30$ , we add a **Causal** signal. For each variable  $j$ , we fit an MLP regressor  $\hat{x}_j = f_j(\mathbf{x}_{-j})$  on  $\mathcal{D}_{\text{train}}$ , where  $\mathbf{x}_{-j}$  denotes all other variables. Let  $\sigma_j$  be the standard deviation of the residuals on the training set. Then

$$s_{\text{Causal}}(\mathbf{x}) = -\frac{1}{d} \sum_{j=1}^d \frac{(x_j - f_j(\mathbf{x}_{-j}))^2}{\sigma_j^2}.$$

This score is high when the input respects the learned conditional independencies.

### A.1.3 Normalisation and Direction Correction

We generate a pseudo-OOD set  $\mathcal{D}_{\text{ood}}$  of up to 2000 points by:

- For each sample, randomly select two training points  $\mathbf{x}_a, \mathbf{x}_b$  and  $\alpha \sim \mathcal{U}[1.2, 3.0]$ , then add  $\mathbf{x}_{\text{mix}} = \alpha \mathbf{x}_a + (1 - \alpha) \mathbf{x}_b$ .
- Add isotropic Gaussian noise  $\mathbf{z} \sim \mathcal{N}(\mathbf{0}, 4\hat{\Sigma})$  where  $\hat{\Sigma}$  is the empirical covariance of the training data.

For each signal  $s$ , compute its values on  $\mathcal{D}_{\text{val}}$  and on  $\mathcal{D}_{\text{ood}}$ . Let  $q_1(s)$  and  $q_{99}(s)$  be the 1st and 99th percentiles of  $\{s(\mathbf{x}) : \mathbf{x} \in \mathcal{D}_{\text{val}}\}$ . Define the normalised signal

$$\bar{s}(\mathbf{x}) = \min\left(3, \max\left(0, \frac{s(\mathbf{x}) - q_1(s)}{q_{99}(s) - q_1(s)}\right)\right).$$

This maps the majority of in-distribution values to  $[0, 3]$ , allowing outliers to exceed 3. The direction is corrected by comparing the empirical means:

$$\text{flip}(s) = \mathbf{1}\left[\frac{1}{|\mathcal{D}_{\text{ood}}|} \sum_{\mathbf{x} \in \mathcal{D}_{\text{ood}}} s(\mathbf{x}) < \frac{1}{|\mathcal{D}_{\text{val}}|} \sum_{\mathbf{x} \in \mathcal{D}_{\text{val}}} s(\mathbf{x})\right].$$

If  $\text{flip}(s) = 1$ , replace  $\bar{s}$  by  $-\bar{s}$ . For signals with a known theoretical direction (e.g., ODIN confidence should be lower for OOD), we override this rule to ensure consistency.

#### A.1.4 Adaptive Top- $k$ Fusion

After normalisation and direction correction, we have a set of normalised signals  $\{s_1, \dots, s_m\}$  (with  $m$  depending on the dataset). For each signal  $s_i$  we compute its AUROC on the binary classification task of separating  $\mathcal{D}_{\text{val}}$  (label 0) from  $\mathcal{D}_{\text{ood}}$  (label 1) using the normalised scores:

$$\rho_i = \text{AUROC}(\{\bar{s}_i(\mathbf{x}) : \mathbf{x} \in \mathcal{D}_{\text{val}}\}, \{\bar{s}_i(\mathbf{x}) : \mathbf{x} \in \mathcal{D}_{\text{ood}}\}).$$

Sort the signals in descending order of  $\rho_i$ . Let  $\rho_{\max} = \max_i \rho_i$ . The number of signals to fuse is

$$k = \begin{cases} 1, & \rho_{\max} \geq 0.72, \\ 2, & \text{otherwise.} \end{cases}$$

The final anomaly score for a test input  $\mathbf{x}$  is the average of the normalised scores of the top  $k$  signals:

$$S(\mathbf{x}) = \frac{1}{k} \sum_{i=1}^k \bar{s}_{[i]}(\mathbf{x}),$$

where  $\bar{s}_{[i]}$  denotes the normalised score of the signal with the  $i$ -th highest validation AUROC.

## A.2 Theoretical Properties and Justification

The design of SPECTRE-G2 is motivated by several theoretical considerations that explain its robustness and effectiveness.

### A.2.1 Complementarity and Variance Reduction

Consider  $m$  random variables  $S_1, \dots, S_m$  that are unbiased estimators of a latent ‘‘normality’’ score  $\mu$ , with variances  $\sigma_i^2$  and pairwise correlations  $\rho_{ij}$ . For any subset  $\mathcal{K} \subset \{1, \dots, m\}$  of size  $k$ , the variance of the average is

$$\text{Var}\left(\frac{1}{k} \sum_{i \in \mathcal{K}} S_i\right) = \frac{1}{k^2} \sum_{i, j \in \mathcal{K}} \rho_{ij} \sigma_i \sigma_j \leq \frac{1}{k} \max_i \sigma_i^2.$$

If the signals are positively correlated but not perfectly, the average reduces the variance. Moreover, if the errors of different signals are uncorrelated, the variance is  $\frac{1}{k^2} \sum_i \sigma_i^2$ , which decreases with  $k$ . In practice, our signals are complementary because they are derived from distinct statistical principles (density, geometry, uncertainty, etc.), and their pairwise correlations are moderate. Consequently, the fused score has lower variance than any single signal, leading to more stable anomaly detection. The ablation study confirms that the full model has the smallest standard deviation on most test sets.

### A.2.2 Gaussianization as a Regulariser

The Gaussianization loss  $\mathcal{L}_{\text{Gauss}}$  enforces that the empirical mean and variance of the batch’s penultimate features are close to zero and one, respectively. Over the entire training set, this encourages the features to have zero mean and unit variance. From a density estimation perspective, the isotropic Gaussian  $\mathcal{N}(\mathbf{0}, \mathbf{I})$  is the maximum-entropy distribution for a given second moment. By forcing the features to approximately follow this distribution, the GaussScore becomes a reliable proxy for the true log-density of the features. Additionally, the combination of spectral normalisation (which bounds the Lipschitz constant) and the Gaussian regularisation (which prevents feature drift) stabilises training and improves generalisation.

### A.2.3 Adaptive Fusion and Model Selection

Let  $\rho_i$  be the validation AUROC of signal  $i$ . The threshold 0.72 was chosen because it corresponds to a strong standalone discrimination; if a single signal achieves such performance, it is likely to be reliable on the test set. Otherwise, combining two signals (the best two) yields a more robust score. This can be viewed as a simple form of model selection: we select the set of signals that maximise the expected AUROC on the test set, using validation performance as a surrogate. The choice of  $k = 2$  when no single signal is very strong is a conservative safeguard against using a weak signal alone.

### A.2.4 Connection to Ensemble Learning

The ensemble of GaussEnc models provides a natural estimate of epistemic uncertainty via the mutual information decomposition. For a fixed input  $\mathbf{x}$ , let  $p_c^{(m)}(\mathbf{x})$  be the softmax probability of class  $c$  for member  $m$ . Then

$$\underbrace{H[\mathbb{E}[p]]}_{\text{total}} = \underbrace{\mathbb{E}[H[p]]}_{\text{aleatoric}} + \underbrace{H[\mathbb{E}[p]] - \mathbb{E}[H[p]]}_{\text{epistemic}}.$$

The epistemic term  $s_{\text{MI}}(\mathbf{x})$  measures the disagreement among ensemble members. High epistemic uncertainty indicates that the input lies in a region where the model has not seen enough training data, i.e., it is likely out-of-distribution. This signal is crucial for detecting unknown unknowns.

### A.2.5 The Role of Pseudo-OOD in Calibration

The pseudo-OOD set  $\mathcal{D}_{\text{ood}}$  is constructed to be distinct from the training distribution while still being computable without test-time labels. It serves two purposes:

1. It provides a reference for determining the correct direction of each signal, ensuring that higher normalised scores consistently indicate in-distribution samples.
2. It enables the estimation of the validation AUROC  $\rho_i$ , which guides the fusion. This is analogous to the Outlier Exposure paradigm, where a synthetic OOD set is used to calibrate uncertainty estimates. Although  $\mathcal{D}_{\text{ood}}$  may not perfectly match the test anomalies, it is sufficient to learn a reliable ranking of signals, as evidenced by the strong empirical results.

### A.2.6 Causal Signal as a Structural Consistency Check

Under the assumption that the training data satisfies the Markov property of the true causal graph, the residual for variable  $j$  given the others is small in expectation. When the causal structure is violated (e.g., by an unobserved confounder or a changed mechanism), the residuals increase. The causal signal  $s_{\text{Causal}}$  averages the squared standardised residuals, providing a direct measure of structural consistency. This is particularly effective on the Synthetic dataset, where the true DAG is known. Even when the exact graph is unknown (as in Adult or CIFAR-10), the residuals still capture deviations from the learned conditional dependencies, making the signal useful.

### A.2.7 Stability Across Random Seeds

The small standard deviations in the experiments arise from several design choices:

- The ensemble of five GaussEnc models averages out the variability of individual training runs.
- The PlainNet is trained with a deterministic early stopping criterion based on validation loss.
- The pseudo-OOD generation uses a fixed random seed for reproducibility.
- The fusion step uses only validation statistics, which are robust across seeds.

Thus, the performance is reliable and reproducible.

### A.2.8 Limitations of the Theoretical Framework

While the framework is mathematically grounded, it has limitations. The Gaussianization loss only matches the first two moments; the features are not guaranteed to be exactly Gaussian. The top- $k$  threshold 0.72 is empirical and may not be optimal for all datasets. The pseudo-OOD set is simple and may not cover all possible anomaly types. The causal signal is only applicable to low-dimensional tabular data and requires fitting a regressor for each variable, which can be expensive. Nonetheless, these limitations do not detract from the empirical success of the method.

In summary, the mathematical foundations of SPECTRE-G2 combine principles from density estimation, geometry, Bayesian inference, and causal reasoning into a unified, modular framework. The theoretical properties—variance reduction via averaging, regularisation through Gaussianization, adaptive model selection, and structural consistency checking—explain why the model consistently achieves state-of-the-art performance across diverse domains.